Engineering Applications of Artificial Intelligence 101 (2021) 104209

Contents lists available at ScienceDirect

Engineering Applications of Artificial Intelligence

journal homepage: www.elsevier.com/locate/engappai

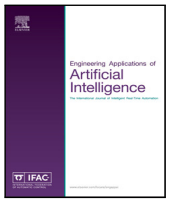

An image segmentation method based on a modified local-information weighted intuitionistic Fuzzy C-means clustering and Gold-panning Algorithm

Dong Wei [a], Zhongbin Wang [a,b,*], Lei Si [a,*], Chao Tan [a], Xuliang Lu [a]

[a] School of Mechatronic Engineering, China University of Mining and Technology, No. 1 Daxue Road, Xuzhou, China
[b] Jiangsu Key Laboratory of Mine Mechanical and Electrical Equipment, China University of Mining and Technology, No. 1 Daxue Road, Xuzhou, China

ARTICLE INFO

Keywords:
Image segmentation
Unsupervised clustering algorithm
Local-information weight
Swarm intelligence

ABSTRACT

The image segmentation method based on clustering analysis has the advantages of small sample space constraints and strong universality. As an unsupervised clustering algorithm, the fuzzy C-means clustering algorithm is widely used in practical engineering. However, it is still some shortcomings: the fuzzy C-means clustering algorithm is difficult to interpret the noise effectively, which makes it more sensitive to the noise, and the selection of key parameters has to be made by trial and error experiments, reducing the adaptability of the algorithm. Besides, its iteration process is heavily influenced by the initial clustering centers and easy to fall into local optimum. Therefore, an intuitionistic Fuzzy C-means clustering method, based on local-information weight, is proposed in this paper. By introducing the local-information weight, the proposed algorithm adjusts the local-information influence weight adaptively in fuzzy partition, which enhances its robustness to noisy images. Furthermore, a novel swarm intelligence algorithm, called the Gold-Panning Algorithm, is proposed to optimize the initial clustering centers and key parameters in the clustering algorithm. By utilizing the Gold-Panning Algorithm, the adaptability of the proposed clustering algorithm is further improved. In this paper, the proposed methods are explained in detail and compared with the existing methods to demonstrate its superior performance.

1. Introduction

In image processing, image segmentation is the process of dividing an image into several regions with unique properties. Its goal is to make the image representation more meaningful and easier to analyze (Gonzales and Richard, 2010). Image segmentation technology has been widely used in biology, medicine, psychology, economics, and industrial engineering.

As an unsupervised learning method, clustering algorithms can effectively solve the problem of lack of prior knowledge in practical engineering. Therefore, the image segmentation method based on clustering algorithms came into being. K-means (Lloyd, 1982) is one of the most commonly clustering algorithms and has been widely used in image segmentation (Mignotte, 2008). However, due to noise and other reasons, traditional hard clustering, such as K-means, is often unable to perform image processing tasks reliably (Yang, 2009). Compared with traditional hard clustering, the fuzzy C-means clustering (FCM) method is more suitable to solve such tasks (Bezdek, 1981), which is widely used in actual engineering (Chuang et al., 2006).

Since the FCM was proposed, many scholars have proposed its variants to improve the performance of the traditional FCM algorithm from different perspectives (Gu et al., 2017; Ahmed et al., 2002; Szilagyi et al., 2003). The intuitionistic fuzzy C-means clustering (IFCM) algorithm, as one of many variants of the FCM, further enlarges the application scope of the fuzzy clustering method with its more accurate membership degree description by introducing new attribute parameters: non-membership degree and hesitancy degree (Zeshui and Junjie, 2010). The IFCM successfully describes the uncertainty of fuzzy events, but it is susceptible to noise due to the lack of local information (Verma et al., 2016). In 2010, Krinidis, S. and Chatzis, V. suggested the fuzzy local information C-Means (FLICM) clustering algorithm to solve such a problem successfully (Krinidis and Chatzis, 2010). By introducing local information into the original FCM, the capacity of the FLICM to resist noise has been greatly enhanced. However, the introduction of local information will have an impact on the original fuzzy partition. Besides, during the imaging process, due to the different performance of sensor units, the noise generated in the imaging process is often non-uniform, a typical example is infrared thermal imaging (Bai et al., 2016), so it is inadequate to evaluate the influence of local information on membership degree with the same weight. Therefore, a local-information weighted intuitionistic fuzzy C-means (LWIFCM) clustering algorithm

* Corresponding authors.
E-mail addresses: wangzbpaper@126.com (Z. Wang), sileicool@163.com (L. Si).

https://doi.org/10.1016/j.engappai.2021.104209
Received 29 October 2019; Received in revised form 15 December 2020; Accepted 16 February 2021
Available online 3 March 2021

is proposed in this paper. In the LWIFCM, local-information weight is introduced to balance the influence of local information on the fuzzy partition, which makes the influence of local information increase in high noise areas, but decrease in low noise areas.

Moreover, as a supplement to the clustering algorithm, swarm intelligence algorithms have been increasingly used to optimize the key parameters of the clustering algorithm and select initial clustering centers (Zhide et al., 2009; Ichihashi et al., 2008). Through multiple iterations, the classification methods based on fuzzy clustering will select better initial clustering centers, eliminating the randomness and making the obtained results more accurate and stable. Meanwhile, the optimized parameters will bring more accurate clustering results. In recent years, influenced by the rapid development of artificial intelligence, swarm intelligence has attracted more and more attention from scholars. Kennedy, J. et al. proposed the particle swarm optimization (PSO) in 1995, which simulates the individuals' movement of birds flock (Kennedy and Eberhart, 1995). Because of the excellent ability of the PSO in dealing with practical problems, many scholars have been attracted to further study it (Tanweer et al., 2015; Wang et al., 2017). Since the PSO was proposed, swarm intelligence algorithms based on other animal behavior have been proposed in succession. The ant colony optimization algorithm (ACO) (Dorigo, 1992) and artificial bee colony algorithm (ABC) (Karaboga, 2010) imitate the behavior of ants and bees, respectively. The main idea of the ACO, ABC and their improved variants (Xue et al., 2018; Zhang and Wong, 2018) is to achieve the approximation to the optimal position through information exchange between different individuals. Inspired by the echolocation behavior of bats, the bat algorithm (BA) is a metaheuristic algorithm for global optimization, which was proposed by Xin-She Yang in 2010 (Yang, 2010b). To some extent, the BA combines the main advantages of the PSO and the harmony search, making it have a better optimization ability than both. Therefore, the BA and its variants (Tsai et al., 2012; Saad et al., 2019) are also widely used in many optimization problems. In addition to the algorithms mentioned above, many other swarm algorithms also show excellent optimization ability in practical applications, such as the bacterial foraging optimization algorithm (BFOA) (Passino, 2002), fruit fly optimization algorithm (FOA) (Pan, 2012, 2013, 2014), etc. Aiming at the problems that the fuzzy clustering methods are greatly influenced by the initial clustering centers and there is no uniform standard for setting key parameters, swarm intelligence methods can solve such problems adaptively and further improve the performance of clustering methods. Therefore, simulating the social behavior of gold diggers, a novel swarm intelligence algorithm, called Gold-Panning Algorithm (GPA), is proposed to supplement the proposed clustering algorithm to enhance the adaptability in image segmentation. In the GPA, each individual is affected by all other individuals to varying degrees in iterative updates, instead of blindly obeying several elite individuals in the current iteration. At the same time, each individual makes decisions on his/her behavior, rather than just following the established behavior rules. Such equality relationship between individuals makes the algorithm more easily step out from the local optimum to improve the convergence accuracy of the algorithm.

The rest of this paper is organized as follows. The core idea and implementation of the LWIFCM are detailed in Section 2. In Section 3, a novel swarm intelligence algorithm is proposed to further optimize the proposed fuzzy clustering algorithm, and compared with other existing algorithms through simulations to verify its superiority in the image segmentation application. In Section 4, the proposed fuzzy clustering algorithm is applied to solve the problem of coal–rock interface recognition, which proves its application ability in practical engineering. And concluding remarks are provided in Section 5.

2. Local-information weighted intuitionistic Fuzzy C-means clustering algorithm

2.1. Fuzzy C-means clustering

Among fuzzy clustering algorithms, the Fuzzy C-Means (FCM) algorithm is the most widely used and successful. It obtains the membership degree of data points to clustering centers by optimizing the objective function $J(U,V)$, to determine the class of the data points to achieve the purpose of automatic classification of the sample data. Its basic definition can be presented as follows:

$$J(U,V)=\sum_{i}^{c}\sum_{j}^{n}{u_{i,j}}^{m}d^2(x_j,v_i), \tag{1}$$

where the object x_j belongs to sample set $X=\{x_1,x_2,\ldots,x_N\}$, $c\rightarrow[1,N]$ is the number of cluster, N is the number of sample data, $u_{i,j}$ is the membership degree of x_j in the ith cluster, m is the fuzzifier constant, $d(x_j,v_i)$ is a distance measure between object x_j and cluster center v_i. The outline of the FCM clustering algorithm are depicted in the following:

Step 1: Set the values of m, c, N and the accuracy of the objective function ε,

Step 2: Initialization of fuzzy partition matrix U,

Step 3: Updating fuzzy partition matrix U and cluster center V by Eqs. (2) (3)

$$u_{i,j}=1/\sum_{k}^{c}\left[d^2(x_j,v_i)/d^2(x_j,v_k)\right]^{2/(m-1)}, \tag{2}$$

$$v_i=(\sum_{j=1}^{N}{u_{ij}}^{m}x_j)/\sum_{j=1}^{N}{u_{ij}}^{m}, \tag{3}$$

Step 4: if $|J(t)-J(t+1)|<\varepsilon$ then stop, otherwise, repeat Step 3.

2.2. Variants of Fuzzy C-means clustering algorithm

2.2.1. Intuitionistic Fuzzy C-mean clustering algorithm

The intuitionistic fuzzy sets (IFS) (Atanasov, 1986), as an important extension of the fuzzy sets, delicately characterize the fuzzy nature of the objective world by adding new attribute parameters: non-membership degree γ and uncertainty degree π. The IFS A on the set X is defined as:

$$A=\{u_A(x),\gamma_A(x),\pi_A(x)|\forall x\in X\}, \tag{4}$$

where $u_A(x)\rightarrow[0,1]$, $\gamma_A(x)\rightarrow[0,1]$ and $0\leq u_A(x)+\gamma_A(x)\leq 1$. And the uncertainty degree can be defined as $\pi_A(x)=1-u_A(x)-\gamma_A(x)$. In particular, when $\pi_A(x)=1-u_A(x)$, intuitionistic fuzzy set A becomes ordinary fuzzy set.

Zadeh first used the concept of the intuitionistic fuzzy entropy (IFE) to measure the fuzziness of the fuzzy sets in 1965 (Zadeh, 1965). Later, Kaufmann redefined the concept by measuring the distance (Kaufmann, 1980). Yager defines it as the distance to a cluster and its complement (Yager, 1980). Szmidt and Kacpryzk define entropy (Szmidt and Kacpryzk, 2001) from a non-probabilistic point of view. The intuitionistic fuzzy entropy (IFE) can be defined as:

$$IFE(A)=\sum_{i=1}^{n}\pi_A(x_i)\exp(1-\pi_A(x_i)), \tag{5}$$

According to Yager-generating functions, the non-membership degree can be expressed as

$$\gamma_A(x_i)=(1-u_A(x_i)^{\alpha})^{1/\alpha}, x\in X, \tag{6}$$

where α called uncertainty parameter. Then, the uncertainty degree can be expressed as

$$\pi_A(x_i)=1-u_A(x_i)-(1-u_A(x_i)^{\alpha})^{1/\alpha}, x\in X, \tag{7}$$

Therefore, intuitionistic fuzzy set A can be expressed as:

$$A^{IFS} = [u_A(x_i), (1-u_A(x_i)^{\alpha})^{1/\alpha}, 1-u_A(x_i)-(1-u_A(x_i)^{\alpha})^{1/\alpha} | x \in X], \quad (8)$$

Furthermore, the intuitionistic fuzzy C-mean (IFCM) clustering algorithm is formed by replacing the fuzzy membership degree in the original FCM with the intuitionistic fuzzy membership degree. The objective function $J^*(U,V)$ of the IFCM is defined as

$$J^*(U,V) = \sum_{i}^{c}\sum_{j}^{n} {u_{ij}^*}^m d^2(x_j, v_i) + \sum_{i=1}^{c} \pi_i^* \exp(1-\pi_i^*), \quad (9)$$

where ${u^*_{i,j}}^m = u_{i,j} + \pi_{i,j}$, $\pi_i^* = \sum_{j=1}^{n} \pi_{i,j}, j \in [1, N]$. And the second half of the right side of Eq. (5) is the intuitionistic fuzzy entropy of the sample set. In the IFCM, the updating mode of membership degree U is unchanged, and the one of clustering center V is changed to

$$v_i^* = (\sum_{j=1}^{N} {u_{ij}^*}^m x_k) / \sum_{j=1}^{N} {u_{ij}^*}^m, \quad (10)$$

However, the IFCM clustering algorithm also has its drawbacks that it is too sensitive and vulnerable to noise.

2.2.2. Fuzzy local information C-means clustering algorithm

The fuzzy local information C-means (FLICM) algorithm (Krinidis and Chatzis, 2010) includes a optimization factor G_{ij} (as shown in Eq. (11)) to balance the image details and image noise.

$$G_{ij} = \sum_{k \in N_j, k \neq j} (1-u_{ik})^m \left\| x_j - v_i \right\|^2 / (d_{jk}+1), 1 \le i \le c, 1 \le j \le N, \quad (11)$$

where jth is the center of the local window, and kth is neighboring pixels in the jth window. N_j represents the number of neighboring pixels around the centered pixel x_j. Its optimization objective function is defined as

$$J(U,V) = \sum_{i}^{c}\sum_{j}^{n} {u_{ij}}^m d^2(x_j, v_i) + G_{ij}, \quad (12)$$

In the FLICM clustering algorithm, the implementation process is basically the same as that of the original FCM. And the update equation of fuzzy membership degree becomes:

$$u_{ij} = 1 / \sum_{r=1}^{c} \left(\frac{\left\| x_j - v_i \right\|^2 + G_{ij}}{\left\| x_j - v_r \right\|^2 + G_{ij}} \right)^{-\frac{1}{m-1}}, \quad (13)$$

The FLICM algorithm does not introduce additional parameters, which improves the influence of noise on the fuzzy partition to a certain extent. However, it is obviously not enough to use the same local information application strategy for all pixels in the images with non-uniform noise, which widely exist in practical engineering.

2.3. A local-information weighted intuitionistic Fuzzy C-means clustering algorithm

To overcome the shortcomings of the above algorithms, the local-information weighted intuitionistic Fuzzy C-means (LWIFCM) clustering algorithm is proposed in this section. By introducing the local information weight κ_{ij}, the influencing degree of local information on clustering results is adjusted adaptively, to avoid relying too much on local information in low noise areas and ignoring the influence of membership degree itself. On the contrary, the proposed clustering algorithm can give full play to the role of local information factor G in high noise areas.

In the LWIFCM, the optimization objective function and local information weight κ_{ij} are expressed as

$$\hat{J}(U,V) = \sum_{i}^{c}\sum_{j}^{n} \hat{u}_{ij} d^2(x_j, v_i) + \sum_{i=1}^{c} \pi_i^* \exp(1-\pi_i^*) + \kappa_{ij} G_{ij}, \quad (14)$$

$$\kappa_{ij} = \frac{\sigma_j^2 + \rho}{\overline{\sigma^2} + \rho}, \quad (15)$$

where σ_j^2 is the variance of the sample data in the jth window (same as Eq. (11)), $\overline{\sigma^2}$ is the mean square error of sample data in all windows whose size is the same as the jth window. The definitions of N_j and k are consistent with Eq. (11). And ρ is a small constant to prevent distortion caused by denominator 0, which is selected as $10^{-3}\eta$ (η is the range of gray levels of input images). Moreover, in order to avoid ignoring the effect of original fuzzy membership caused by replacing original fuzzy membership with intuitionistic fuzzy membership, the membership degree is defined in the LWIFCM algorithm as $\hat{u}_{ij} = {u_{i,j}}^m + {u_{ij}^*}^m$.

When the distribution of image noise is not uniform, the parameter κ_{ij} is introduced to balance the influence of the G_{ij}. At the position with strong noise, the value of the κ_{ij} is large, which strengthens the influence of the G_{ij} in Eq. (14), and the surrounding elements can be fully considered, to reduce the influence of noise on the segmentation result when the current front point is greatly affected by noise. On the contrary, in the relatively flat position, the κ_{ij} will limit the effect of the G_{ij} with a small value, to retain the influence of the current point on the segmentation result as much as possible. Therefore, the LWIFCM has better adaptability than the FLICM, which can solve the data clustering more robustly by balancing the G_{ij} influence in whether the strong-noise or flat positions.

3. Modified LWIFCM clustering method based on gold-panning algorithm

For the fuzzy-clustering based segmentation methods, the effects are mainly affected by two aspects: the setting of the key parameters and the selection of initial clustering centers. In the LWIFCM, the key parameters include the fuzzifier constant m and uncertainty parameter α, which are usually determined by trial and error experiments. The selection of initial clustering centers has a great influence on clustering results, which is directly related to the quality of image segmentation. Swarm intelligence algorithms are usually used as a supplement to clustering methods to optimize the performance of the clustering methods and increase adaptability. Inspired by the gold-panning social behaviors, a novel swarm intelligence algorithm, the Gold-Panning Algorithm (GPA), is proposed in this paper which imitates the social behaviors of diggers. The implementation of the GPA and the clustering algorithm based on the GPA (GPA-LWIFCM) is introduced in this section.

3.1. Social behaviors of gold diggers

Gold Rush broke out in the 1940s, causing a large number of gold diggers flocking into California to seek wealth. It is assumed that the social behaviors of gold diggers are as follows:

When the first gold diggers come to the mining area, due to lack of previous experience, they often randomly choose their initial locations for gold panning, built houses, purchase equipment, then officially start their first round of gold panning. It is can be recognized that the gold reserves in the gold-panning sites chosen by the gold diggers will determine their income. When the first round of gold panning is over, each gold digger will get a separate income. First, they communicate with each other, and determine where their income ranks compared with other gold diggers, then make plans for their future. At this time, the lower the income, the easier he/she choose to leave, and the higher the income, the more reluctant to give up the career they have started. But this is not inevitable. Each individual has the right to choose his/her future. When a gold digger leaves, the new one will join and replace the original one to keep the total number of gold diggers unchanged. New gold diggers will also randomly choose initial positions to start their careers due to inexperience. The first gold diggers who choose to stay will select the next round of gold-panning sites according to the current

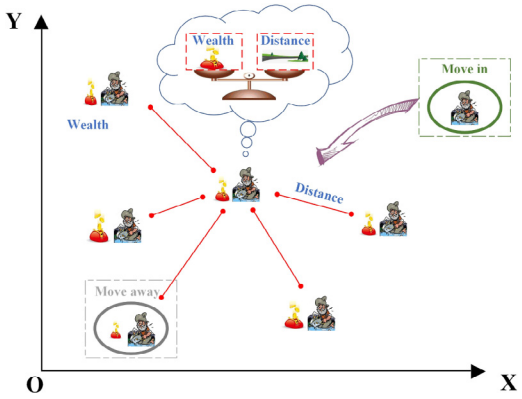

Fig. 1. Illustration of gold-digger social behaviors.

situation. The selection will be constrained by two factors: income and distance. As the income increases, the position of the earner becomes more and more attractive to other gold diggers. However, due to the high cost of long-distance relocation, gold diggers are more willing to choose places close to themselves and with high incomes. Finally, in order to seek higher incomes, each gold digger is willing to take chances near his/her chosen location, and so are those who already have higher incomes. Because everyone wants to have a better life. At this time, a round of gold-panning work officially ended, and then, another round will begin, so the cycle continues.

In conclusion, the social behaviors of gold diggers are an activity tending to the optimal position of gold panning, in which each gold digger has his own ideas and moves to the ideal position according to decision-making in each round. Based on the mentioned social behaviors, the Gold-Panning Algorithm (GPA) is proposed in this paper.

3.2. Implementation of the gold-panning algorithm

In this section, based on behaviors of gold diggers, the following parameters were introduced: the total number of gold diggers (p), the number of iterations (n), the dimensions of the search variables (d) and the wealth tolerance factor (t_w) (see Fig. 1).

With the example of solving the minimum of the objective function, the Gold-Panning Algorithm (GPA) can be divided into the following 7 steps:

Step 1: Initialize the gold diggers' locations randomly and calculate their income value.

$$loc_i = \left(X_i, Y_i, \ldots\right), \tag{16}$$

$$Wealth\,(i) = \text{function}(loc_i), \tag{17}$$

where i represents the ith individual of the p gold diggers.

Step 2: Calculate the wealth weight factor: Firstly, the optimal value and the worst value are calculated in the current iteration.

$$\begin{cases} Max_w = \max(Wealth(i)) \\ Min_w = \min(Wealth(i)), \end{cases} \tag{18}$$

Then, each individual wealth value is normalized to get its wealth weight factor in the current iteration.

$$f_{wealth}(i) = \frac{Wealth(i) - Min_w}{Max_w - Min_w}, \tag{19}$$

Step 3: Make the individual decisions: According to the individual wealth weight factor, each individual's wealth tolerance factor is calculated.

$$t_w(i) = \frac{1}{1 + \exp\left(-k_w \times \left(f_{wealth}(i) - 0.5\right)\right)}, \tag{20}$$

where k_w represent the subjective tolerance factor. By adjusting the k_w value, the corresponding relationship between (t_w) and f_{wealth} can be adjusted.

Then, a random number between 0 and 1 is generated. When it is greater than the wealth tolerance factor (t_w), the gold digger's location remains unchanged. Otherwise, its location is randomly initialized. Next, Update the wealth weight factor.

Step 4: Calculate the distance weight factor: Firstly, assume that the decision-making of gold diggers is not only influenced by the wealth of other diggers, but also inversely proportional to the square of the distance from others. That is to say, the relationship between the selections of a gold digger and the distances (between the gold digger and other individuals) obeys the law of inverse square ratio. Then, the squares of distances between the ith individual and other individuals are calculated. The maximum value is:

$$Max_d(i) = \max(\text{Distance}^2(j \to i)), \quad (j \neq i), \tag{21}$$

where $\text{Distance}^2(j \to i)$ represents the square of the distance between the jth individual and the ith individual. And the minimum distance is the distance between the individual and itself, with a value of 0.

Furthermore, the distance weight factor of each individual relative to the ith individual is calculated (the jth individual is token as an example):

$$f_{distance}(j) = \frac{\text{Distance}^2(j \to i)}{Max_d(i)}, \tag{22}$$

Step 5: Select the ideal position: According to the wealth weight factor and the distance weight factor, the next round of gold-panning location is selected, then the individual moved to it. Moreover, to prevent ill-conditioned results, the sum of the distance weight factor and 1 is used as the denominator.

$$loc_i = loc_i + \sum_{j=1}^{p} \frac{f_{wealth}(j)}{f_{distance}(j) + 1}(loc_j - loc_i), \tag{23}$$

where loc_i and loc_j are the locations of the ith individual and the jth individual, respectively.

Step 6: Explore the better gold-panning position: Explore a local potential solution around the selected ideal position. If the new solution is better than the original solution, the original solution will be updated to the new one, otherwise, the original solution will be retained.

$$loc_i''' = loc_i + 0.01 \times \text{randn}(1, d), \tag{24}$$

$$\begin{matrix} if & \text{function}(loc_i''') \le \text{function}(loc_i), & loc_i = loc_i \\ else & loc_i = loc_i''' & , \end{matrix} \tag{25}$$

Step 7: Record the position and wealth value of the gold diggers who have gained the most wealth in this round. Then, enter iterative optimization to repeat the implementation of steps 2–7.

The pseudo-code of the GPA algorithm is demonstrated in Algorithm 1.

3.3. Validation and comparison of the GPA

The GPA is a swarm intelligence algorithm based on imitating gold-panning social activities. In this section, the simulation results are presented and analyzed to evaluate the performance of the GPA algorithm. To facilitate visualization, we have implemented it using Matlab for various test functions. All of the experiments are carried out on CPU Intel Core i7-6700k PC with 16G memory, the same below.

3.3.1. Typical benchmark functions

Among test functions, 12 typical test functions are chosen, which are widely used in validating new algorithms. And the test functions are shown in Table 1.

Table 1
Test functions.

Functions	Formula	Type	Dimension/Search domain
Ackley	$f(\mathbf{x}) = -20\exp\left(-0.2\sqrt{\frac{1}{d}\sum_{i=1}^{d}x_i^2}\right) - \exp\left(\frac{1}{d}\sum_{i=1}^{d}\cos(2\pi x_i)\right) + 20 + \mathrm{e}$	Many minima	50/ $x_1 \in [-15,-5]$, $x_2 \in [-3,+3]$
Bukin N. 6	$f(\mathbf{x}) = 100\sqrt{\lvert x_2 - 0.01x_1^2\rvert} + 0.01\lvert x_1 + 10\rvert$	Many minima	2/$x_i \in [-5,+5]$
Griewank	$f(\mathbf{x}) = \sum_{i=1}^{d}\frac{x_i^2}{4000} - \prod_{i=1}^{d}\cos\left(\frac{x_i}{\sqrt{i}}\right) + 1$	Many minima	10/$x_i \in [-600,600]$
Levy	$f(\mathbf{x}) = \sin^2(\pi\omega_1) + \sum_{i=1}^{d-1}(\omega_1 - 1)^2[1+ 10\sin^2(\pi\omega_i + 1)] + (\omega_d - 1)^2\left[1 + \sin^2(2\pi\omega_d)\right]$, where $\omega_i = 1 + \frac{x_i - 1}{4}$, for all $i = 1,\ldots,d$	Many minima	30/$x_i \in [-10,10]$
Rotated hyper-ellipsoid	$f(\mathbf{x}) = \sum_{i=1}^{d}\sum_{j=1}^{i}x_j^2$	Bowl-shaped	10/$x_i \in [-65.536,65.536]$
Sphere	$f(\mathbf{x}) = \sum_{i=1}^{d}x_i^2$	Bowl-shaped	50/$x_i \in [-5.12,5.12]$
Booth	$f(\mathbf{x}) = (x_1 + 2x_2 - 7)^2 + (2x_1 + x_2 - 5)^2$	Plate-shaped	2/$x_i \in [-10,10]$
Matyas	$f(\mathbf{x}) = 0.26(x_1^2 + x_2^2) - 0.48x_1x_2$	Plate-shaped	2/$x_i \in [-10,10]$
3-Hump camel	$f(\mathbf{x}) = 2x_1^2 - 1.05x_1^2 + \frac{x_1^2}{6} + x_1x_2 + x_2^2$	Valley-shaped	2/$x_i \in [-5,5]$
Easom	$f(\mathbf{x}) = -\cos(x_1)\cos(x_2)\exp(-((x_1 - \pi)^2 + (x_2 - \pi)^2))$	Steep ridges	2/$x_i \in [-100,100]$
Beale	$f(\mathbf{x}) = (1.5 - x_1 + x_1x_2)^2 + (2.25 - x_1 + x_1x_2^2)^2 + (2.625 - x_1 + x_1x_2^3)^2$	Other	2/$x_i \in [-4.5,4.5]$
Goldstein-price	$f(\mathbf{x}) = [1 + (x_1 + x_2 + 1)^2(19 - 14x_1 + 3x_1^2 - 14x_2 + 6x_1x_2 + 3x_2^2)] \times [30 + (2x_1 - 3x_2)^2(18 - 32x_1 + 12x_1^2 + 48x_2 - 36x_1x_2 + 27x_2^2)]$	Other	2/$x_i \in [-2,2]$

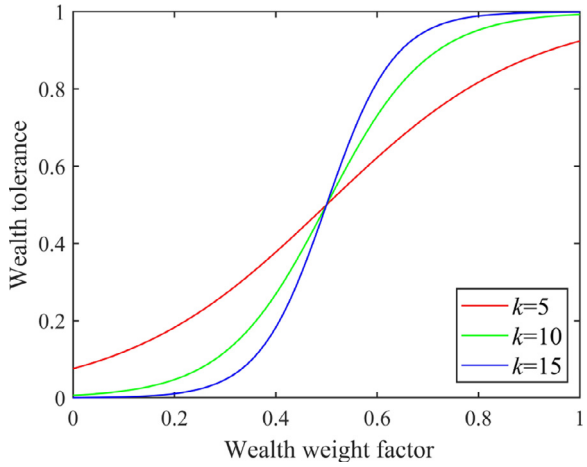

Fig. 2. Illustration of the wealth tolerance factor t_w.

Algorithm 1 The pseudo-code of the Gold-Panning Algorithm

```
Initialize p, n, d, k_w and the objective function f();
Initialize loc_i = (X_i, Y_i, ···),
n = 1
while (n ≤ N)
    Wealth(i) = function(loc_i)
    Calculate f_wealth(i) and t_w(i) according to Eqs. (19), (20)
    if (rand(0,1) ≤ t_w(i))
        loc_i ← loc_i'.   *Random initialize position*
    end if
    Wealth'(i) = function(loc_i)
    Calculate f_distance(i) according to Eq. (22)
    loc_i ← loc_i'' according to Eq. (23).   *Directed update location*
    loc_i ← loc_i''' according to Eq. (24).   *Explore nearby*
    Wealth''(i) = function(loc_i)
    if Wealth''(i) ≥ Wealth'(i)
        Accept loc_i as the optimal.
    end if
    Search the current best location (loc_best) and wealth (Wealth_best)
    n=n+1
end while
return loc_best and Wealth_best
```

3.3.2. Effect of the subjective tolerance factor

The effect of the subjective tolerance factor k_w on the solution quality is presented in Tables 2 and 3. Six test functions, taken from the different types in Table 1, are used. Each test instance is run for 100 iterations and the total number of gold diggers is 20. For each parameter setup, 51 independent runs are carried out. The first column shows the k_w value ranging from 5 to 15. The rest columns show the simulating results including the minima and medians for each selected test function. The best values are shown in bold (same below).

By the Wilcoxon ranked-sum test (Khan and Mahmood, 2019), the p value of the simulation results is 0.0027, which shows that the experimental results of minima and medians are statistically significant. The results are given in Tables 2 and 3 suggest that the choice of k_w value can affect the quality of the solutions. In Table 2, it can be noticed that the best minimum is obtained with $k_w = 15$ for most of the test cases. The exceptions are the cases Sphere and Beale, where the best values are obtained with $k_w = 13$ and 11 respectively. In Table 3, the medians of the minima are obtained with $k_w = 11$ and $k_w = 13$. (The distribution of the solutions can be better reflected by the medians. For example, when $k_w = 15$ and the test function is Ackley, the results of Tables 2 and 3 show that 50% minima are distributed between 5.28E−09 and 3.12E−07.)

The results can be justified as follows: The choice of k_w value will affect the probability of keeping the current position in the iterative process. For example, as shown in Fig. 2, when $f_{wealth} = 1$, if $k_w = 5$, $t_w = 0.9241$, indicating that there is a 92.41% probability of maintaining the current position at this time. If $k_w = 10$ or 15, the probabilities increases to 99.33% and 99.94%, respectively. Correspondingly, when $f_{wealth} = 0$, if $k_w = 5$, 10 or 15, the probabilities of individuals

Table 2
The effect of the subjective tolerance factor k_w on solution quality (minima).

k_w	Ackley	Sphere	Booth	3-Hump camel	Easom	Beale
5	5.87E−08	9.04E−20	9.10E−10	2.35E−11	7.17E−09	3.34E−12
7	3.34E−08	5.31E−20	5.11E−10	5.42E−12	1.21E−09	3.14E−12
9	4.69E−08	2.24E−20	6.87E−10	7.60E−12	1.65E−09	7.70E−12
11	3.45E−08	1.03E−20	2.96E−10	5.94E−12	4.33E−09	**6.32E−13**
13	9.05E−09	**2.87E−21**	1.50E−10	6.56E−11	5.09E−10	5.79E−12
15	**5.28E−09**	1.08E−19	**5.37E−11**	**5.11E−12**	**3.58E−10**	2.59E−12

Table 3
The effect of the subjective tolerance factor k_w on solution quality (medians).

k_w	Ackley	Sphere	Booth	3-Hump camel	Easom	Beale
5	3.96E−07	2.40E−17	2.00E−07	1.14E−10	3.99E−07	5.57E−04
7	3.98E−07	3.90E−17	2.11E−08	1.23E−10	3.65E−07	6.05E−05
9	3.23E−07	3.54E−17	3.96E−08	1.09E−10	3.71E−07	5.16E−06
11	3.91E−07	3.51E−17	3.10E−08	8.73E−10	**1.64E−07**	3.52E−06
13	**2.98E−07**	**1.50E−17**	**2.17E−08**	**1.08E−10**	3.03E−07	**9.67E−07**
15	3.12E−07	3.62E−17	4.98E−08	1.69E−10	4.18E−07	1.83E−06

being randomly initialized are 7.59%, 0.67% and 0.06%, respectively. This shows that with the increase of k_w value, the better solution is more likely to be retained, and the worse solution is more likely to be discarded. This leads to a more probability of the individuals concentrate on the better position in the current iteration. Therefore, the iterative direction of the algorithm is clearer, and the accuracy of the best minimum is higher in 51 independent runs. The introduction of the worse results provides an additional perturbation for the algorithm, which makes the algorithm have a strong ability to break away from local optimization. When the worse results are discarded in large quantities, this ability will decline, which also logically confirms the results in Tables 2 and 3. Thus, the selection of k_w can affect the solution quality of the proposed algorithm. Moreover, numbers of experiments show that when k_w is selected between 10 and 13, the accuracy and convergence rate are better for most issues.

3.3.3. Effect of the colony size

Tables 4 and 5 show the effect of the colony size, i.e. the total number of gold diggers, in the experiments on the solution quality. The selection of test functions, number of iterations and number of independent runs are consistent with Section 3.3.2. The comparison of colony size is done assuming $k_w = 13$. The first column shows the total number of gold diggers ranging from 10 to 30. The rest columns show the simulating results including the minima and medians for each selected test function.

The results are validated using the Wilcoxon ranked-sum test ($p = 0.0005$), showing using the minima and the medians is statistically significant in evaluating the effect of the colony size. The results given in Tables 4 and 5 suggest that the solution quality can be improved by increasing the colony size. Almost all the test functions get good results when the colony size increases. The medians prove that the quality of the solution can be improved by increasing the size of the colony from the perspective of the accuracy distribution of the solution. For example, for Ackley, when $p = 20$, 50% minima are distributed between 1.15E−08 and 8.97E−08, but when $p = 30$, 50% minima are distributed between 9.62E−09 and 7.26E−08. Compared with $p = 20$, when $p = 30$, the algorithm converges to a higher precision interval.

3.3.4. Comparison of the GPA with other algorithms

The GPA algorithm is compared with other 10 swarm intelligence optimization algorithms in this section. These algorithms include the dynamic particle swarm optimization algorithm (DPSO) (Liu et al., 2016), the firefly algorithm (FA) (Yang, 2010a), the improved fruit fly optimization algorithm (IFOA) (Jing et al., 2016), the modified bat algorithm (MBA) (Jing et al., 2018), the harris hawks optimization algorithm (HHO) (Heidari et al., 2019), the moth-flame optimization algorithm (MFO) (Mirjalili, 2015), the gray wolf optimizer (GWO) (Mirjalili et al., 2014), the multi-verse optimizer (MVO) (Mirjalili et al., 2016), the whale optimization algorithm (WOA) (Mirjalili and Lewis, 2016), and the salp swarm algorithm (SSA) (Mirjalili et al., 2017). Each test instance is run for 100 iterations, 101 independent runs are carried out. To have a fair comparison, the population size of all algorithms involved in the experiment is set to 20. For the GPA, the subjective tolerance factor k_w is set to 13.

The DPSO is a variant of the PSO, which improves the original algorithm from two aspects: Firstly, Liu and Wei designed a novel movement update equation to enhance the dynamic performance of the PSO; Secondly, proposed a dynamic OBL using adaptive Gaussian-distribution to overcome the blindness in the p_{best} search. According to Liu et al. (2016), the parameters of the DPSO are set as follows: the acceleration constants $c_1 = c_2 = 1.49445$, the adjustment parameter $\lambda = 6$, and the opposition learning probability ($Oc = 0.38$). The inertia weight ω is set on [0.90, 0.40] and decreases linearly.

The FOA is a kind of interactive evolutionary computation method by imitating foraging behavior of the fruit fly individuals and populations, which proposed in 2012. The IFOA is an improved algorithm based on the standard FOA, which replaces the original random fly distance range FR obeying uniform distribution ($FR \sim U(-L, L)$) with the one obeying normal distribution ($FR \sim N(0, L^2)$), where L named as step size. In the experiment, the step sizes L of the IFOA is set to 10% of the dynamic range of the variable on each dimension to ensure strong optimization ability in different test functions.

Both the FA and BA are proposed by Professor Xin-She Yang of Cambridge University. The inspiration of the FA comes from the behavior of firefly flicker. Each firefly is attracted to other fireflies, rather than following a single leader, which makes the FA not easy to premature. According to Qi et al. (2017), its parameters are set as follows: the attraction coefficient base value ($\beta_0 = 1$), the light absorption coefficient ($\gamma = 1$) and the mutation coefficient ($\alpha_0 = 1$).

The MBA is an improvement of the BA. By introducing the interference coefficient and improving the search strategy based on the standard BA, the ability to escape the present extremum is enhanced. The key parameters of the MBA are set as follows: the range of pulse loudness $A \in [0, 2]$, the range of emission frequency $r \in [0, 1]$, the range of pulse frequency $f \in [0, 2]$, the attenuation coefficient of loudness $a = 0.9$, the enhancement coefficient of emission frequency $g = 0.9$, and the disturbance coefficient $c = 10$. (The above parameters are the optimal parameter settings selected through multiple tests.)

Mirjalili and his team proposed a number of excellent optimization algorithms in recent years, including the HHO, MFO, GWO, MVO, WOA, and SSA. Each algorithm proposed by him or his team has its own advantages and gives excellent solutions to many problems. In this section, the parameters of the above algorithm are set as follows: In the HHO, set $\beta = 1.5$ in the Levy flight. In the MFO, set the spiral factor $b = 1$ and the convergence constant a linearly decreasing from −1 to −2

Table 4
The effect of the colony size p on solution quality (minima).

p	Ackley	Sphere	Booth	3-Hump camel	Easom	Beale
10	2.00E−08	1.91E−20	9.91E−09	7.42E−11	1.37E−09	5.92E−08
15	1.12E−08	1.60E−19	7.45E−10	4.33E−11	6.02E−10	6.36E−10
20	1.15E−08	8.43E−20	3.01E−10	1.25E−11	4.33E−10	1.43E−11
25	1.08E−08	3.75E−21	3.02E−10	5.24E−12	3.95E−10	3.30E−12
30	**9.62E−09**	**6.50E−22**	**9.10E−11**	**1.20E−12**	**9.91E−11**	**1.26E−12**

Table 5
The effect of the colony size p on solution quality (medians).

p	Ackley	Sphere	Booth	3-Hump camel	Easom	Beale
10	9.40E−08	6.38E−17	9.71E−07	4.44E−10	8.75E−07	4.94E−06
15	9.02E−08	5.79E−17	3.51E−08	2.81E−10	3.86E−07	2.12E−06
20	8.97E−08	5.14E−17	2.14E−08	9.36E−11	1.90E−07	9.14E−07
25	7.93E−08	3.42E−17	1.89E−08	7.76E−12	9.25E−08	9.88E−07
30	**7.26E−08**	**3.02E−17**	**5.49E−09**	**5.86E−12**	**7.04E−08**	**2.87E−08**

according to Mirjalili (2015). In the GWO, set the convergence constant a decreasing linearly from 2 to 0 according to Mirjalili et al. (2014). In the MVO, set the minimum and maximum of the wormhole existence probability $WEP_{min} = 0.2$ and $WEP_{max} = 1$ according to Mirjalili et al. (2016). In the WOA and SSA, no additional parameters are required, and all equations are set in the same way as the ones in Mirjalili and Lewis (2016) and Mirjalili et al. (2017).

Table 6 show the results obtained for the 11 algorithms concerning each optimization objective, and the optimal and sub-optimal values of different function optimization results are bold and italicized respectively, to make a distinction. Fig. 3 shows the optimization curves of the 11 algorithms when they reach the median minimum values for 6 typical functions in different kinds of types (In order to show the convergence accuracy of the algorithms more intuitively, parameter $OptimalAccuracy$ is defined in Eq. (26)):

$$OptimalAccuracy = \log_{10}(OptimalValue), \tag{26}$$

In addition, the results are statistically validated through the Wilcoxon ranked-sum test, in order to test whether the optimization performance of proposed algorithm is significant. If the rank-sum of the GPA results is smaller than others', it is recorded as "+", otherwise recorded as "−". Moreover, it is assumed that the significance level α is 0.05. If the p value is less than 0.05, it is recorded as "Y"; if it is greater than 0.05, it is recorded as "N". The test results are recorded in Table 7.

Table 6 show that the GPA obtains the best comprehensive performances and have significant advantages compared with most of the typical test functions for the five evaluation indicators. However, compared with the HHO, MFO, GWO, and WOA, the optimization ability for the Sphere function needs to be further improved. Besides, the HHO also obtains the significant best results for Griewank, Rotated Hyper-Ellipso, and 3-hump camel functions. It can be seen that the optimization performance of the HHO is stronger than the GPA for the bowl-shaped and similar bowl-shaped test functions. But the accuracy stability of the HHO is unsatisfactory, and it indicates that the robustness is an important advantage of the GPA compared with the HHO. In conclusion, for most of the 12 typical test functions, the GPA achieves the significantly optimal results, but compared with the algorithms like the HHO, the optimization ability of the bowl-shaped functions is slightly insufficient.

Further, as can be seen in Fig. 3, the convergence speed of the GPA is close to or even faster than other algorithms. This behavior appears to be logical due to the properties of the GPA. In the GPA, all the gold diggers can explore the optimal value independently, and realize individual motion according to mutual information interaction. Moreover, because of the existence of self-decision (according to Eq. (23)), these movements have the directionality, and then accelerate the convergence efficiency of the algorithm.

On the basis of the above evaluation, in order to analyze the optimization performance of the proposed algorithm more comprehensively, the 29 functions on the 30D in the CEC'17 (shown in Table 8) were used to further evaluate the proposed algorithm in this section. Moreover, in order to evaluate the performances more convincingly, the effective butterfly optimizer with covariance matrix adapted retreat phase (EBOwithCMAR) (Kumar et al., 2017), which showed excellent performances in the CEC'17, was introduced to replace the IFOA that had performed poorly in the previous simulations. In the EBOwithCMAR, the parameters are consistent with those in Kumar et al. (2017): For the EBO, $PS_{1,max} = 18D = 540$, $PS_{1,min} = 4$, $PS_{2,max} = 46.8D = 1404$, $PS_{2,min} = 10$, $H = 6$. For the CMAR, $PS_3 = 4 + (3\ln(D)) = 14$, and $\sigma = 0.3$. Besides, $CS = 200$. For local search, $prob_{ls} = 0.1$ and $cfe_{ls} = 0.25 \times FE_{max} = 12{,}500$. Each test instance is run for 50,000 iterations, and 51 independent runs are carried out. For each algorithm, the parameter settings are consistent with the previous. Median, average value and standard deviation of the function error values are recorded in Table 9 (Within each cell, the median, average value, and standard deviation are represented from top to bottom). As mentioned above, the Wilcoxon ranked-sum test is also used to evaluate the significance of the algorithm performance. The difference is that, in addition to the Wilcoxon ranked-sum test, the Fridman test was added to show the ranking of the optimization abilities for the algorithms more obviously.

By comprehensively analyzing the statistical data in Tables 9 and 10, the following conclusions can be drawn: the GPA is superior to the other algorithms for most of the CEC'17 test functions, both in terms of accuracy and algorithm robustness. The exceptions are results for the F2 (lost to the SSA), F3 (lost to the EBOwithCMAR), F5 (lost to the GWO, MVO and SSA), F8 (lost to the EBOwithCMAR), F14 (lost to the MVO), F18 (lost to the MVO), F23 (lost to the DPSO, GWO, MVO, and SSA), F26 (lost to the MVO), and F27 (lost to the EBOwithCMAR), a total of 14 combinations (in 290 combinations). However, for the 14 combinations, only 6 combinations show significant advantages comparing with the GPA, which is the F3/EBOwithCMAR, F5/MVO, F5/GWO, F8/EBOwithCMAR, F14/MVO and F18/MVO. In Table 11, the Friedman test was utilized to rank the results of the 11 algorithms, and the results showed that: except F2, F3, F5, F8, F14, F18, F23, F26, and F27, the GPA obtained the best results, which is consistent with the results used by the Wilcoxon ranked-sum test. The Fridman test results show that the GPA shows the best comprehensive performance for 29 CEC'17 test functions. The suboptimal was the MVO, and the SSA and EBOwithCMAR come next. It is worth mentioning that the HHO and MFO can also achieve high accuracy in several independent runs. However, their unsatisfactory stabilities make them show no statistical advantages, but their occasional performances are still impressive.

The above results can be logically explained as follows. The advantage of the GPA is that the individuals does not tend to the location of a single optimal solution in each iteration, but comprehensively considers the wealth value of all individuals and the distance from

Table 6
Comparison of the GPA with the DSPO, FA, IFOA, MBA, HHO, MFO, GWO, MVO, WOA, and SSA for 12 typical test functions.

	DPSO	FA	IFOA	MBA	HHO	MFO	GWO	MVO	WOA	SSA	GPA
Functions						Ackley					
MIN	4.10E−05	1.92E−04	3.18E−03	1.05E−04	**2.22E−11**	2.59E−09	7.99E−11	6.07E−03	9.73E−11	2.00E−06	4.40E−08
MED	8.50E−04	2.18E−03	3.60E−03	1.81E−03	**2.46E−08**	5.75E−06	1.11E−07	1.79E−01	9.90E−06	1.54E−05	3.24E−07
MAX	3.26E−02	2.58E+00	3.88E−03	3.57E+00	1.18E−03	2.58E−03	6.08E−05	5.04E−01	3.57E+00	3.57E+00	**7.32E−07**
AVG	2.39E−03	2.79E−02	3.61E−03	2.41E−01	2.20E−05	6.71E−04	3.11E−06	1.77E−01	8.67E−02	1.27E−01	**3.30E−07**
STD	4.49E−03	2.55E−01	1.18E−04	7.72E−01	1.33E−04	3.69E−04	9.59E−06	1.06E−01	5.02E−02	6.02E−01	**1.50E−07**
Functions						Bukin N.6					
MIN	1.96E−10	2.97E−08	4.03E−01	1.61E−08	7.64E−10	**1.54E−12**	2.22E−08	3.17E−05	1.07E−09	8.59E−11	6.05E−12
MED	2.28E−06	3.18E−06	9.97E−01	5.39E−06	4.73E−05	5.23E−03	1.30E−05	2.33E−01	4.24E−01	4.01E−01	**1.32E−06**
MAX	4.22E−03	5.99E−01	5.08E+00	1.16E+00	9.72E+00	1.32E+00	7.93E−01	5.38E+00	8.57E−01	1.03E+00	**1.20E−05**
AVG	7.95E−05	1.78E−02	1.34E+00	1.42E−01	1.36E−01	1.47E−01	9.02E−02	3.37E−01	3.00E−01	3.22E−01	**2.11E−06**
STD	4.30E−04	1.02E−01	9.49E−01	3.06E−01	9.69E−01	2.52E−01	2.18E−01	6.32E−01	2.63E−01	2.75E−01	**2.19E−06**
Functions						Griewank					
MIN	2.19E−03	3.23E−06	3.23E−06	2.24E−05	1.87E−10	2.24E−01	1.19E−05	1.04E−01	**2.36E−07**	9.43E−02	4.18E−06
MED	2.08E−02	1.12E−05	1.12E−05	8.02E−05	**4.87E−09**	6.28E−01	7.48E−02	4.01E−01	4.24E−06	4.07E−01	4.98E−06
MAX	6.64E−02	1.98E−05	1.98E−05	1.13E−02	**2.12E−09**	2.67E+00	3.70E−01	7.57E−01	1.15E+00	1.01E+00	6.21E−06
AVG	2.27E−02	1.15E−05	1.15E−05	6.28E−04	**4.88E−09**	6.99E−01	1.09E−01	4.03E−01	2.35E−01	4.43E−01	4.98E−06
STD	1.12E−02	3.20E−06	3.20E−06	1.70E−03	**2.96E−09**	3.66E−01	8.25E−02	1.46E−01	3.40E−01	1.88E−01	3.71E−07
Functions						Levy					
MIN	1.80E−03	4.56E−03	2.57E−03	9.37E−04	**2.39E−07**	4.17E+00	6.43E−03	2.78E+00	1.67E−03	1.20E+00	7.43E−05
MED	2.46E−03	1.72E−02	2.67E−03	1.85E−03	**2.84E−04**	9.25E+00	6.58E−02	7.38E+00	2.73E−03	3.20E+00	3.39E−04
MAX	3.20E−03	4.05E−02	2.73E−03	2.83E−03	5.87E−03	1.40E+01	3.86E+00	1.23E+01	5.35E+00	7.66E+00	**7.72E−04**
AVG	2.44E−03	1.77E−02	2.66E−03	1.87E−03	6.97E−04	9.19E+00	2.03E−01	7.32E+00	8.41E−02	3.39E+00	**3.50E−04**
STD	3.01E−04	7.85E−03	**3.39E−05**	2.93E−04	1.07E−03	1.95E+00	5.12E−01	2.01E+00	5.43E−01	1.25E+00	1.60E−04
Functions						Rotated hyper-ellipsoid					
MIN	7.51E−02	1.96E−03	1.65E−04	7.74E−04	**1.82E−09**	1.97E+01	1.78E−04	1.73E+00	3.77E−06	1.96E+01	1.12E−05
MED	8.30E−01	5.14E−03	2.00E−04	4.36E−03	**1.24E−07**	2.49E+02	3.40E−03	1.36E+01	9.92E−05	6.74E+02	4.74E−05
MAX	4.06E+00	9.65E−03	2.39E−04	1.02E+00	**5.26E−05**	2.01E+04	1.25E−01	5.75E+01	8.64E−04	4.45E+03	7.77E−05
AVG	9.48E−01	5.17E−03	1.99E−04	3.70E−02	**1.83E−05**	1.30E+03	8.51E−03	1.72E+01	2.76E−05	1.16E+03	4.65E−05
STD	6.57E−01	1.44E−03	1.55E−05	1.18E−01	7.79E−05	2.97E+03	1.49E−02	1.26E+01	1.02E−04	1.15E+03	**1.26E−05**
Functions						Sphere					
MIN	8.71E−17	4.38E−14	3.22E−07	3.52E−14	1.49E−28	2.87E−25	6.13E−30	6.61E−10	**4.05E−30**	1.01E−17	3.26E−20
MED	2.52E−11	5.71E−11	4.04E−07	2.04E−10	1.18E−26	1.38E−23	3.03E−24	5.71E−06	**8.83E−27**	1.75E−13	1.15E−17
MAX	9.22E−08	4.41E−09	4.88E−07	4.61E−09	5.07E−16	1.70E−13	**1.16E−16**	8.50E−04	7.15E−15	1.31E−11	6.38E−15
AVG	1.83E−09	2.43E−10	4.05E−07	6.93E−10	1.08E−16	1.68E−15	**1.15E−18**	4.31E−05	7.08E−17	7.01E−13	5.33E−17
STD	9.49E−09	5.36E−10	3.11E−08	1.05E−09	6.31E−16	1.68E−14	**1.15E−17**	1.09E−04	7.08E−16	1.61E−12	9.83E−16
Functions						Booth					
MIN	6.78E−10	5.57E−10	1.50E+00	3.14E−08	5.55E−06	9.17E−12	2.75E−08	9.04E−06	2.06E−04	**5.73E−13**	3.45E−10
MED	7.94E−06	2.43E−06	1.75E+01	3.15E−06	1.90E−02	3.32E−01	3.25E−05	5.29E−03	5.00E−01	**1.87E−10**	2.76E−08
MAX	3.74E−03	**9.73E−06**	4.52E+01	1.19E+01	4.04E+00	7.82E+02	2.33E−04	4.43E−02	1.63E+01	5.65E+02	4.84E−05
AVG	1.81E−04	2.64E−06	1.74E+01	3.67E−01	3.50E−01	2.83E+02	5.12E−05	7.69E−03	1.54E+00	9.19E+01	**8.71E−07**
STD	5.42E−04	2.15E−06	1.05E+01	1.51E+00	7.36E−01	3.97E+02	4.89E−05	7.62E−03	3.13E+00	2.04E+02	**5.13E−06**
Functions						Matyas					
MIN	1.25E−11	2.05E−09	2.79E−08	3.89E−10	6.66E−15	8.16E−16	**1.13E−17**	1.79E−06	6.83E−13	7.94E−14	2.89E−12
MED	2.17E−08	5.82E−08	3.52E−08	3.60E−08	7.28E−10	4.68E−04	8.65E−10	1.83E−04	4.71E−12	**4.23E−12**	6.16E−10
MAX	5.67E−05	4.20E−07	4.46E−08	4.39E−07	5.82E−08	4.84E+01	1.02E−06	1.98E−03	5.18E−08	2.40E−04	**6.33E−09**
AVG	1.05E−06	8.42E−08	3.55E−08	6.81E−08	7.42E−09	5.90E−01	3.36E−08	2.77E−04	9.37E−09	3.37E−06	**1.04E−09**
STD	5.77E−06	8.28E−08	2.97E−09	8.41E−08	5.95E−09	4.79E+00	1.30E−07	3.09E−04	6.21E−09	2.48E−05	**1.18E−09**
Functions						3-Hump Camel					
MIN	3.49E−11	4.20E−09	2.48E−06	8.48E−09	**4.17E−26**	2.85E−19	2.64E−27	9.13E−05	3.06E−15	1.48E−12	3.25E−11
MED	1.34E−07	7.77E−07	3.17E−06	4.68E−07	1.65E−15	1.69E−14	**2.32E−18**	1.92E−03	2.99E−01	9.31E−11	9.10E−11
MAX	8.64E−05	2.99E−01	4.00E−06	2.99E−01	**6.06E−09**	2.99E−01	2.99E−01	2.23E−02	3.03E−01	2.99E−01	8.41E−08
AVG	2.36E−06	5.91E−03	3.17E−06	1.18E−02	**1.27E−10**	3.25E−02	8.75E−03	3.11E−03	1.54E−01	2.96E−02	1.40E−08
STD	9.27E−06	4.16E−02	2.65E−07	5.82E−02	**6.85E−10**	9.30E−02	5.00E−02	3.84E−03	1.49E−01	8.92E−02	1.32E−08
Functions						Easom					
MIN	9.39E−10	9.39E−09	1.00E+00	1.41E−09	9.04E−08	1.56E−09	2.62E−07	3.26E−04	1.31E−06	**7.15E−13**	4.63E−10
MED	9.93E−07	1.11E−06	1.00E+00	6.32E−07	2.23E−03	1.00E+00	4.40E−05	1.00E+00	1.00E+00	1.00E+00	**3.69E−07**
MAX	3.97E−04	1.00E+00	1.00E+00	1.00E+00	1.00E+00	1.00E+00	1.00E+00	1.00E+00	1.00E+00	1.00E+00	**3.02E−04**
AVG	1.89E−05	4.95E−02	1.00E+00	2.24E−02	5.24E−02	8.41E−01	3.49E−02	8.82E−01	7.54E−01	6.63E−01	**7.88E−06**
STD	6.00E−05	2.17E−01	6.03E−06	1.41E−01	1.94E−01	3.54E−01	1.77E−01	3.22E−01	4.13E−01	4.73E−01	**3.99E−05**
Functions						Beale					
MIN	1.96E−10	2.97E−08	4.03E−01	1.61E−08	7.64E−10	**1.54E−12**	2.22E−08	3.17E−05	1.07E−09	8.59E−11	6.05E−12
MED	2.28E−06	3.18E−06	9.97E−01	5.39E−06	4.73E−05	5.23E−03	1.30E−05	2.33E−01	4.24E−01	4.01E−01	**1.32E−06**
MAX	4.22E−03	5.99E−01	5.08E+00	1.16E+00	9.72E+00	1.32E+00	7.93E−01	5.38E+00	8.57E−01	1.03E+00	**1.20E−05**
AVG	7.95E−05	1.78E−02	1.34E+00	1.42E−01	1.36E−01	1.47E−01	9.02E−02	3.37E−01	3.00E−01	3.22E−01	**2.11E−06**
STD	4.30E−04	1.02E−01	9.49E−01	3.06E−01	9.69E−01	2.52E−01	2.18E−01	6.32E−01	2.63E−01	2.75E−01	**2.19E−06**

(*continued on next page*)

Table 6 (*continued*).

	DPSO	FA	IFOA	MBA	HHO	MFO	GWO	MVO	WOA	SSA	GPA
Functions						Goldstein-price					
MIN	3.42E−08	4.78E−06	5.98E+02	4.21E−06	2.34E−07	5.68E−08	2.90E−06	1.14E−02	3.61E−07	8.42E−09	**6.97E−09**
MED	4.76E−05	1.80E−04	5.98E+02	1.45E−04	6.40E−02	1.42E−07	1.52E−02	9.70E−01	2.71E+01	**9.23E−09**	2.63E−06
MAX	2.53E+00	1.38E−03	5.98E+02	8.10E+01	3.64E+01	6.65E+02	1.08E+02	1.54E+03	1.21E+02	4.06E+00	**2.14E−05**
AVG	2.56E−02	2.69E−04	5.98E+02	4.28E+00	1.01E+01	9.71E+00	1.10E+00	7.31E+01	3.40E+00	5.11E−02	**3.91E−06**
STD	2.50E−01	2.60E−04	4.45E−02	1.19E+01	1.32E+01	6.69E+01	1.07E+01	2.46E+02	1.50E+01	4.14E−01	**4.18E−06**

Table 7
Results of the Wilcoxon ranked-sum test for 12 typical test functions.

GPA vs	DPSO	FA	IFOA	MBA	HHO	MFO	GWO	MVO	WOA	SSA
Ackley	+/Y	+/Y	+/Y	+/Y	+/Y	+/Y	+/Y	+/Y	+/Y	+/Y
Bukin N. 6	+/Y	+/Y	+/Y	+/Y	+/Y	+/Y	+/Y	+/Y	+/Y	+/Y
Griewank	+/Y	+/Y	+/Y	+/Y	−/Y	+/Y	+/Y	+/Y	+/Y	+/Y
Levy	+/Y	+/Y	+/Y	+/Y	+/Y	+/Y	+/Y	+/Y	+/Y	+/Y
Rotated hyper-ellipso	+/Y	+/Y	+/Y	+/Y	−/Y	+/Y	+/Y	+/Y	+/Y	+/Y
Sphere	+/N	+/Y	+/Y	+/Y	−/Y	−/N	−/Y	+/Y	−/Y	+/Y
Booth	+/Y	+/Y	+/Y	+/Y	+/Y	+/Y	+/Y	+/Y	+/Y	+/Y
Matyas	+/Y	+/Y	+/Y	+/Y	+/Y	+/Y	+/Y	+/Y	+/Y	+/Y
3-hump camel	+/Y	+/Y	+/Y	+/Y	−/Y	+/Y	+/Y	+/Y	+/Y	+/Y
Easom	+/Y	+/Y	+/Y	+/Y	+/Y	+/Y	+/Y	+/Y	+/Y	+/Y
Beale	+/Y	+/Y	+/Y	+/Y	+/Y	+/Y	+/Y	+/Y	+/Y	+/Y
Goldstein-price	+/N	+/Y	+/Y	+/Y	+/Y	+/Y	+/Y	+/Y	+/Y	+/Y

Table 8
Summary of the CEC'17 test functions.

	No.	Functions	$F_i^* = \mathrm{F}_i(x^*)$
Unimodal functions	1	Shifted and rotated bent cigar function	100
	2	Shifted and rotated Zakharov function	200
Simple multimodal functions	3	Shifted and rotated Rosenbrock's function	300
	4	Shifted and rotated Rastrigin's function	400
	5	Shifted and rotated expanded Scaffer's F6 function	500
	6	Shifted and rotated Lunacek Bi_Rastrigin function	600
	7	Shifted and rotated non-continuous Rastrigin's function	700
	8	Shifted and rotated Levy function	800
	9	Shifted and rotated Schwefel's function	900
Hybrid functions	10	Hybrid function 1 (N = 3)	1000
	11	Hybrid function 2 (N = 3)	1100
	12	Hybrid function 3 (N = 3)	1200
	13	Hybrid function 4 (N = 4)	1300
	14	Hybrid function 5 (N = 4)	1400
	15	Hybrid function 6 (N = 5)	1500
	16	Hybrid function 6 (N = 5)	1600
	17	Hybrid function 6 (N = 5)	1700
	18	Hybrid function 6 (N = 6)	1800
	19	Hybrid function 6 (N = 6)	1900
Composition functions	20	Composition function 1 (N = 3)	2000
	21	Composition function 2 (N = 3)	2100
	22	Composition function 3 (N = 4)	2200
	23	Composition function 4 (N = 4)	2300
	24	Composition function 5 (N = 5)	2400
	25	Composition function 6 (N = 5)	2500
	26	Composition function 7 (N = 6)	2600
	27	Composition function 8 (N = 6)	2700
	28	Composition function 9 (N = 3)	2800
	29	Composition function 10 (N = 3)	2900
Search range: $[-100, 100]^D$			

themselves, to make individual self-decision (according to Eq. (23)). The existence of self-decision makes the algorithm not easy to fall into the local optimum and avoid the premature maturity of the algorithm. Moreover, the core idea of the GPA is similar to the FA algorithm, where each individual is attracted to other individuals rather than following a single leader, but there are still obvious differences. In the FA, each firefly is attracted by other fireflies whose light intensities are greater than its own, and the distance it moves is a function of the attractiveness (β), which is only related to the distance between the fireflies. In contrast, in the GPA, the movement direction and distance of each gold digger are related to the obtained wealth and distance from herself/himself of all gold diggers. Through the wealth weight factor (f_{wealth}) and the distance weight factor ($f_{distance}$), each gold digger decides about her/his ideal position in current iteration. By introducing the wealth tolerance factor (t_w), each gold digger is more likely to approach the optimal position. Meanwhile, the gold digger with less wealth retained by small probability will become the disturbance in the next iteration, to ensure the ability to escape from the localization trap in the whole iteration process. Moreover, the retained diggers do small-scale random exploration around their ideal position, which further enhances the ability of local optimization. Random location initialization of the new diggers in each iteration also guarantees the global optimization ability of the algorithm.

Moreover, the algorithm complexity according to Kumar et al. (2017) is shown in Table 12. T_0 is the time assessed by running the

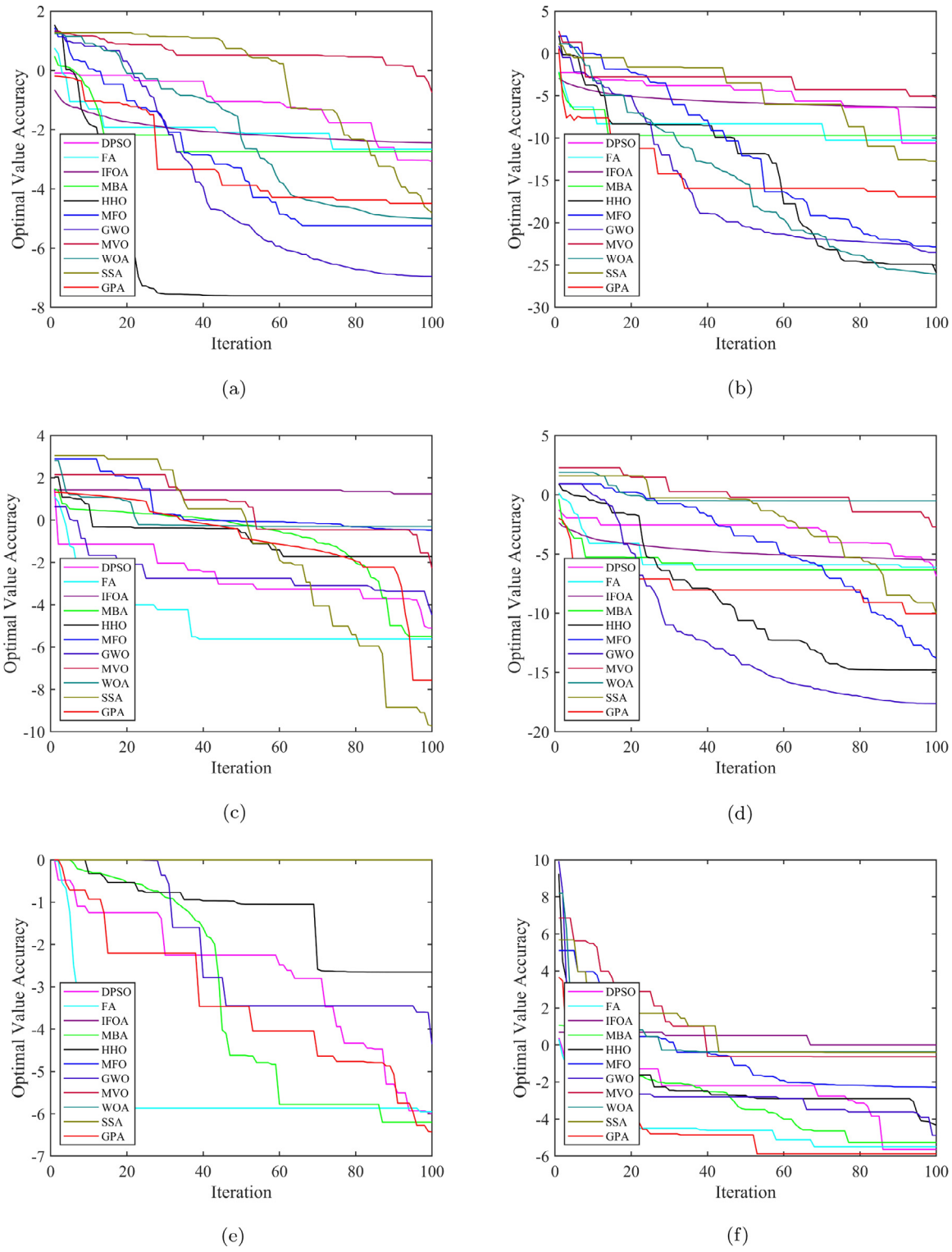

Fig. 3. Comparison of the GPA with other algorithms. (a) Ackley; (b) Sphere; (c) Booth; (d) 3-hump camel; (e) Easom; (f) Beale.

following test problem:

$x = 0.55;$
$for\ i = 1 : 1000000$
$x = x + x; x = x/2; x = x * x; x = sqrt(x);$
$x = \log(x); x = \exp(x); x = x/(x + 2);$
end

T_1 is the time to execute for CEC'17 benchmark function F18 for 200,000 objective function evaluations while T_2 is the time to execute the mentioned algorithms with 200,000 objective function evaluations of F18 in D dimensions. T_2 is calculated for 5 independent runs, and $\hat{T}_2$ denotes the mean of T_2. Finally, the algorithm complexity is expressed by the linear growth of $(\hat{T}_2 - T_1)/T_0$. It can be seen, the algorithm complexity of the GPA is close to that of the MFO and GWO, second

Table 9
Comparison of the GPA with the DPSO, FA, MBA, HHO, MFO, GWO, MVO, WOA, EBOwithCMAR and SSA for CEC'17.

	DPSO	FA	MBA	HHO	MFO	GWO	MVO	WOA	SSA	EBOwithCMAR	GPA
	2.56E+01	1.99E+02	6.10E−03	5.85E+01	5.63E−05	1.25E−04	2.71E−05	8.70E−04	1.37E−05	1.98E−05	**6.59E−07**
F1	2.65E+01	1.99E+02	6.14E−03	5.77E+01	1.62E+00	5.57E−01	4.21E−05	4.98E−03	2.16E−05	3.61E−04	**6.38E−07**
	1.62E+01	1.42E−13	1.26E−03	3.51E+01	4.17E+00	1.36E+00	3.85E−05	1.17E−02	2.31E−05	1.56E−03	**1.56E−07**
	6.81E+02	1.91E+03	2.58E−01	1.18E+03	9.95E+02	6.80E+01	3.95E−04	3.20E+01	**1.48E−10**	1.75E−07	2.37E−10
F2	7.66E+02	1.91E+03	2.58E−01	1.18E+03	1.73E+03	3.04E+02	4.26E−04	8.61E+01	**1.38E−10**	2.45E−06	2.36E−10
	4.43E+02	**2.19E−11**	5.03E−02	4.59E+02	2.08E+03	3.96E+02	2.14E−04	1.46E+02	7.72E−11	9.66E−06	7.79E−11
	3.15E+04	8.01E+05	4.61E+02	5.66E+04	2.86E+03	1.92E+03	4.77E+02	2.01E+03	7.25E+02	**3.99E+00**	2.34E+01
F3	3.71E+04	8.01E+05	1.82E+03	7.92E+04	8.01E+03	5.38E+03	4.54E+02	8.78E+03	6.08E+02	**2.58E+01**	6.33E+01
	2.61E+04	6.66E−10	4.51E+03	6.25E+04	1.02E+04	4.88E+03	2.22E+02	9.64E+03	2.88E+02	**2.89E+01**	2.42E+02
	8.72E+01	1.05E+02	1.42E+02	6.45E+01	2.76E+01	1.45E+01	1.28E+01	5.03E+01	1.45E+01	9.95E+00	**5.24E+00**
F4	8.63E+01	1.04E+02	1.44E+02	6.70E+01	2.94E+01	1.43E+01	1.29E+01	4.74E+01	1.57E+01	1.31E+01	**5.36E+00**
	2.14E+01	5.90E+00	5.36E+01	2.24E+01	1.06E+01	6.42E+00	5.53E+00	2.00E+01	8.12E+00	6.77E+00	**1.91E+00**
	7.60E−01	8.72E−01	1.38E+00	8.14E−01	7.16E−02	1.60E−02	**5.22E−03**	4.91E−01	5.95E−02	5.87E−02	6.47E−02
F5	7.54E−01	8.73E−01	1.38E+00	7.86E−01	1.27E−01	1.65E−02	**1.58E−02**	5.04E−01	7.89E−02	6.57E−02	6.54E−02
	2.00E−01	3.34E−02	3.62E−01	2.27E−01	1.39E−01	**1.93E−02**	3.25E−02	2.41E−01	8.05E−02	3.39E−02	2.06E−02
	1.14E+02	9.23E+01	7.86E+02	1.34E+02	4.66E+01	3.69E+01	3.02E+01	1.04E+02	3.50E+01	3.83E+01	**2.36E+01**
F6	1.27E+02	1.43E+02	1.10E+03	1.91E+02	7.61E+01	6.68E+01	5.11E+01	1.76E+02	5.03E+01	4.17E+01	**3.60E+01**
	1.26E+02	3.45E+02	2.01E+03	4.05E+02	1.69E+02	2.02E+02	1.40E+02	5.36E+02	8.87E+01	**9.67E+00**	3.14E+01
	3.96E+01	3.31E+01	1.34E+02	4.21E+01	3.18E+01	1.50E+01	1.49E+01	3.68E+01	1.79E+01	9.95E+00	**6.02E+00**
F7	4.05E+01	3.39E+01	1.35E+02	4.14E+01	3.44E+01	1.57E+01	1.44E+01	3.92E+01	1.87E+01	1.10E+01	**5.95E+00**
	7.59E+00	3.32E+00	4.59E+01	1.03E+01	1.35E+01	5.84E+00	6.94E+00	1.31E+01	7.94E+00	5.26E+00	**2.23E+00**
	3.42E+01	4.40E+01	2.88E+02	5.04E+01	1.92E+01	6.60E−01	1.62E−05	2.30E+01	3.06E−02	**0.00E+00**	8.77E−06
F8	3.82E+01	4.42E+01	3.05E+02	4.68E+01	3.17E+01	1.84E+00	5.42E−03	2.75E+01	5.95E−02	**5.27E−03**	1.31E−02
	1.90E+01	6.00E+00	1.30E+02	1.67E+01	3.55E+01	2.79E+00	**1.31E−02**	2.14E+01	1.03E−01	2.13E−02	3.06E−02
	9.67E+02	1.15E+03	9.52E+02	8.80E+02	6.74E+02	3.46E+02	3.97E+02	7.37E+02	4.70E+02	7.72E+02	**3.16E+02**
F9	1.04E+03	1.21E+03	9.87E+02	8.83E+02	7.31E+02	3.86E+02	4.23E+02	7.21E+02	4.85E+02	7.59E+02	**3.04E+02**
	2.51E+02	1.93E+02	2.72E+02	2.06E+02	2.70E+02	1.85E+02	1.73E+02	2.24E+02	1.73E+02	**1.32E+02**	1.38E+02
	2.67E+02	1.99E+05	2.43E+02	4.16E+02	1.55E+02	4.27E+01	1.77E+01	9.23E+01	5.69E+01	1.89E+01	**1.41E+01**
F10	3.18E+02	1.99E+05	3.02E+02	1.00E+03	2.53E+02	1.70E+02	1.87E+01	1.46E+02	6.22E+01	2.76E+01	**1.49E+01**
	1.94E+02	7.47E+00	2.10E+02	1.32E+03	4.40E+02	8.62E+02	8.66E+00	1.19E+02	3.46E+01	2.24E+01	**6.75E+00**
	7.10E+01	1.70E+05	1.52E+03	2.16E+04	**1.37E+02**	1.77E+03	1.87E+02	9.19E+03	1.65E+02	1.33E+03	4.32E+02
F11	2.68E+02	1.70E+05	1.81E+03	5.30E+04	1.91E+04	3.85E+03	4.99E+02	1.79E+04	2.29E+03	**1.73E+02**	4.63E+02
	4.88E+02	**1.64E+00**	1.04E+03	8.20E+04	3.27E+04	4.32E+03	1.05E+03	2.34E+04	2.85E+03	7.33E+01	2.96E+01
	1.70E+01	2.11E+04	3.79E+01	1.77E+01	1.65E+01	1.31E+01	**1.04E+01**	1.61E+01	1.62E+01	2.75E+03	1.29E+01
F12	2.91E+01	2.11E+04	4.60E+01	2.04E+01	2.45E+01	2.10E+01	1.83E+01	1.96E+01	1.92E+01	3.01E+03	**1.76E+01**
	2.61E+01	**2.72E−02**	4.71E+01	1.48E+01	1.52E+01	1.36E+01	7.39E+00	1.50E+01	9.39E+02	1.49E+01	1.39E+01
	5.28E+01	5.99E+08	6.48E+01	6.37E+01	1.01E+03	4.40E+01	**1.35E+01**	6.66E+01	3.81E+01	3.24E+01	2.40E+01
F13	7.73E+01	5.99E+08	9.03E+01	8.23E+01	2.13E+03	6.03E+02	3.37E+01	1.77E+02	3.97E+01	3.71E+01	**2.48E+01**
	7.26E+01	**2.52E+00**	8.59E+01	5.14E+01	3.44E+03	8.40E+02	4.28E+01	4.20E+02	1.29E+01	1.91E+01	1.21E+01
	9.60E+01	1.20E+07	3.18E+02	1.77E+03	1.31E+03	2.09E+02	**3.22E+00**	4.25E+02	6.47E+01	3.89E+01	5.63E+00
F14	1.50E+02	1.20E+07	4.46E+02	1.56E+03	1.93E+03	4.73E+02	**3.71E+00**	6.54E+02	6.94E+01	3.99E+01	6.36E+00
	1.74E+02	**1.54E+00**	3.93E+02	9.15E+02	1.99E+03	4.41E+02	2.02E+00	6.26E+02	7.60E+00	4.86E+01	4.04E+00
	3.13E+02	5.76E+02	5.48E+02	3.28E+02	2.10E+02	9.95E+01	1.09E+02	1.77E+02	**1.84E+01**	5.07E+01	3.01E+01
F15	3.29E+02	5.77E+02	5.34E+02	3.02E+02	2.02E+02	1.22E+02	1.50E+02	1.89E+02	5.53E+01	4.99E+01	**2.87E+01**
	1.31E+02	4.85E+01	2.10E+02	1.28E+02	1.19E+02	1.07E+02	1.20E+02	1.08E+02	7.06E+01	2.43E+01	**1.31E+01**
	2.48E+02	2.89E+02	1.02E+03	2.81E+02	2.02E+02	1.28E+02	1.01E+02	1.87E+02	1.18E+02	1.93E+02	**2.58E+01**
F16	2.95E+02	2.95E+02	1.09E+03	2.86E+02	2.69E+02	1.41E+02	1.60E+02	2.02E+02	1.46E+02	2.05E+02	**3.29E+01**
	1.58E+02	**9.01E+00**	5.36E+02	1.33E+02	2.00E+02	7.29E+01	1.51E+02	9.13E+01	8.45E+01	7.24E+01	2.26E+01
	5.35E+01	1.45E+08	7.17E+02	1.51E+02	3.66E+02	4.03E+02	1.23E+02	2.07E+02	2.64E+02	9.82E+01	**1.78E+01**
F17	2.80E+01	1.45E+08	9.59E+02	2.08E+02	3.92E+02	4.08E+02	1.67E+02	2.62E+02	2.93E+02	9.74E+01	**2.80E+01**
	1.12E+02	**1.31E−01**	9.70E+02	1.97E+02	2.57E+02	2.59E+02	1.41E+02	2.04E+02	2.09E+02	3.14E+01	2.69E+01
	2.04E+01	1.57E+09	3.43E+01	2.04E+03	5.46E+02	1.67E+01	**1.55E+00**	1.86E+03	9.59E+00	3.64E+01	9.61E+00
F18	9.36E+01	1.57E+09	1.80E+02	1.31E+04	2.24E+03	1.33E+03	**1.70E+00**	4.03E+03	1.44E+01	3.92E+01	1.08E+01
	1.57E+02	6.66E−01	4.33E+02	3.76E+04	3.58E+03	3.90E+03	**6.22E−01**	6.72E+03	1.47E+01	1.17E+01	6.76E+00
	3.24E+02	5.23E+02	6.10E+02	2.76E+02	1.48E+02	**7.27E+01**	1.76E+02	2.07E+02	8.12E+01	2.32E+02	9.69E+01
F19	3.05E+02	5.30E+02	5.96E+02	2.67E+02	1.77E+02	1.19E+02	1.62E+02	2.14E+02	1.05E+02	2.26E+02	**1.01E+02**
	6.99E+01	**3.23E+01**	2.33E+02	1.11E+02	1.02E+02	7.80E+01	9.50E+01	9.37E+01	6.88E+01	1.05E+02	4.36E+01
	2.79E+02	4.66E+02	3.37E+02	2.54E+02	2.31E+02	2.16E+02	2.16E+02	2.35E+02	1.04E+02	2.10E+02	**1.00E+02**
F20	2.60E+02	4.64E+02	3.32E+02	2.37E+02	2.25E+02	2.10E+02	2.02E+02	2.02E+02	1.56E+02	2.05E+02	**1.23E+02**
	6.34E+01	4.26E+00	4.09E+01	5.70E+01	3.27E+01	3.36E+01	4.17E+01	6.54E+01	6.21E+01	**3.17E+01**	5.20E+01
	5.64E+02	1.87E+03	1.77E+03	5.50E+02	1.11E+02	1.05E+02	1.03E+02	1.13E+02	1.04E+02	**1.01E+02**	1.08E+02
F21	6.72E+02	1.87E+03	1.64E+03	6.54E+02	1.54E+02	1.38E+02	1.86E+02	3.19E+02	1.22E+02	**1.01E+02**	1.16E+02
	4.57E+02	5.30E+01	6.92E+02	5.55E+02	1.95E+02	1.59E+02	2.26E+02	5.06E+02	1.88E+02	**8.09E−01**	1.01E+02
	5.68E+02	1.06E+03	5.86E+02	4.68E+02	3.97E+02	3.75E+02	3.77E+02	4.10E+02	3.76E+02	3.71E+02	**3.57E+02**
F22	5.89E+02	1.09E+03	5.91E+02	4.75E+02	3.98E+02	3.77E+02	3.79E+02	4.12E+02	3.78E+02	3.70E+02	**3.60E+02**
	1.18E+02	6.04E+01	8.41E+01	4.71E+01	1.36E+01	9.20E+00	8.86E+00	2.32E+01	**7.09E+00**	1.11E+01	9.27E+00

(*continued on next page*)

Table 9 (*continued*).

	DPSO	FA	MBA	HHO	MFO	GWO	MVO	WOA	SSA	EBOwithCMAR	GPA
	2.32E+02	7.75E+02	5.26E+02	4.29E+02	3.70E+02	3.45E+02	3.48E+02	3.83E+02	3.43E+02	4.46E+02	3.76E+02
F23	**2.77E+02**	7.75E+02	5.40E+02	4.32E+02	3.70E+02	3.46E+02	3.49E+02	3.68E+02	3.35E+02	4.34E+02	2.80E+02
	1.30E+02	5.58E−01	7.85E+01	8.37E+01	**1.06E+01**	1.21E+01	1.07E+01	7.09E+01	4.83E+01	5.94E+01	1.57E+02
	5.56E+02	1.51E+03	4.44E+02	6.51E+02	4.51E+02	4.34E+02	4.44E+02	4.50E+02	4.44E+02	**4.11E+02**	4.22E+02
F24	5.90E+02	1.51E+03	4.26E+02	6.76E+02	4.52E+02	4.29E+02	4.26E+02	4.20E+02	4.28E+02	4.13E+02	**3.99E+02**
	1.35E+02	3.08E−01	4.72E+01	1.79E+02	3.94E+01	**1.77E+01**	2.25E+01	8.22E+01	2.27E+01	1.81E+01	5.33E+01
	1.60E+03	2.20E+03	2.21E+03	1.65E+03	4.28E+02	3.75E+02	**3.00E+02**	8.82E+02	**3.00E+02**	9.66E+02	**3.00E+02**
F25	1.47E+03	2.20E+03	2.16E+03	1.55E+03	6.01E+02	5.22E+02	4.80E+02	1.02E+03	3.23E+02	7.16E+02	**3.04E+02**
	5.44E+02	9.63E+01	6.65E+02	4.09E+02	3.75E+02	3.98E+02	3.87E+02	6.12E+02	1.58E+02	4.75E+02	**2.80E+01**
	5.00E+02	1.07E+03	5.00E+02	5.21E+02	3.98E+02	3.95E+02	**3.90E+02**	4.11E+02	3.93E+02	4.07E+02	3.92E+02
F26	4.84E+02	1.06E+03	4.85E+02	5.18E+02	3.98E+02	4.06E+02	**3.91E+02**	4.38E+02	3.93E+02	4.06E+02	3.93E+02
	3.28E+01	3.65E+01	3.29E+01	7.35E+01	4.70E+00	1.94E+01	2.95E+00	4.57E+01	2.99E+00	4.94E+00	**1.81E+00**
	5.00E+02	1.24E+03	5.00E+02	7.76E+02	6.03E+02	6.12E+02	5.84E+02	6.12E+02	**3.00E+02**	**3.00E+02**	**3.00E+02**
F27	4.97E+02	1.24E+03	4.91E+02	7.61E+02	5.66E+02	5.65E+02	4.99E+02	5.98E+02	3.48E+02	3.13E+02	**3.06E+02**
	5.57E+00	**1.09E−12**	2.25E+01	2.09E+02	1.21E+02	1.12E+02	1.41E+02	1.71E+02	1.23E+02	3.60E+01	7.61E+01
	5.84E+02	3.50E+03	7.30E+02	5.29E+02	3.64E+02	2.78E+02	2.89E+02	4.21E+02	2.71E+02	2.81E+02	**2.65E+02**
F28	6.48E+02	3.53E+03	7.45E+02	5.17E+02	3.69E+02	3.00E+02	3.13E+02	4.34E+02	2.73E+02	2.88E+02	**2.65E+02**
	2.26E+02	1.10E+02	2.47E+02	1.27E+02	6.80E+01	5.58E+01	6.88E+01	9.07E+01	**3.53E+00**	3.68E+01	6.45E+00
	9.97E+03	1.96E+08	2.07E+03	2.72E+06	7.43E+05	4.52E+04	3.24E+04	2.51E+05	1.10E+04	3.91E+03	**3.99E+02**
F29	5.25E+04	1.96E+08	8.95E+03	4.53E+06	6.37E+05	6.50E+05	4.95E+05	7.08E+05	1.74E+05	3.93E+03	**1.74E+03**
	1.68E+05	9.59E−08	1.53E+04	6.74E+06	5.49E+05	9.48E+05	5.60E+05	9.60E+05	4.26E+05	**3.92E+02**	4.18E+03

Table 10
Results of the Wilcoxon ranked-sum test for CEC'17.

GPA vs	DPSO	FA	MBA	HHO	MFO	GWO	MVO	WOA	SSA	EBOwithCMAR
F1	+/Y	+/Y	+/Y	+/Y	+/Y	+/Y	+/Y	+/Y	+/Y	+/Y
F2	+/Y	+/Y	+/Y	+/Y	+/Y	+/Y	+/Y	+/Y	−/N	+/Y
F3	+/Y	+/Y	+/Y	+/Y	+/Y	+/Y	+/Y	+/Y	+/Y	−/Y
F4	+/Y	+/Y	+/Y	+/Y	+/Y	+/Y	+/Y	+/Y	+/Y	+/Y
F5	+/Y	+/Y	+/Y	+/Y	+/Y	−/Y	−/Y	+/Y	−/N	+/N
F6	+/Y	+/Y	+/Y	+/Y	+/Y	+/Y	+/Y	+/Y	+/Y	+/Y
F7	+/Y	+/Y	+/Y	+/Y	+/Y	+/Y	+/Y	+/Y	+/Y	+/Y
F8	+/Y	+/Y	+/Y	+/Y	+/Y	+/Y	+/Y	+/Y	+/Y	−/Y
F9	+/Y	+/Y	+/Y	+/Y	+/Y	+/Y	+/Y	+/Y	+/Y	+/Y
F10	+/Y	+/Y	+/Y	+/Y	+/Y	+/Y	+/Y	+/Y	+/Y	+/Y
F11	+/Y	+/Y	+/Y	+/Y	+/Y	+/Y	+/Y	+/Y	+/Y	+/Y
F12	+/Y	+/Y	+/Y	+/Y	+/Y	+/Y	+/N	+/Y	+/Y	+/Y
F13	+/Y	+/Y	+/Y	+/Y	+/Y	+/Y	+/Y	+/Y	+/Y	+/Y
F14	+/Y	+/Y	+/Y	+/Y	+/Y	+/Y	−/Y	+/Y	+/Y	+/Y
F15	+/Y	+/Y	+/Y	+/Y	+/Y	+/Y	+/Y	+/Y	+/N	+/N
F16	+/Y	+/Y	+/Y	+/Y	+/Y	+/Y	+/Y	+/Y	+/Y	+/Y
F17	+/Y	+/Y	+/Y	+/Y	+/Y	+/Y	+/Y	+/Y	+/Y	+/Y
F18	+/Y	+/Y	+/Y	+/Y	+/Y	+/Y	−/Y	+/Y	+/N	+/Y
F19	+/Y	+/Y	+/Y	+/Y	+/Y	+/Y	+/Y	+/Y	+/Y	+/Y
F20	+/Y	+/Y	+/Y	+/Y	+/Y	+/Y	+/Y	+/Y	+/N	+/Y
F21	+/Y	+/Y	+/Y	+/Y	+/Y	+/Y	+/Y	+/Y	+/Y	+/N
F22	+/Y	+/Y	+/Y	+/Y	+/Y	+/Y	+/Y	+/Y	+/Y	+/Y
F23	−/N	+/Y	+/Y	+/Y	+/N	−/N	−/N	+/N	−/N	+/Y
F24	+/Y	+/Y	+/Y	+/Y	+/Y	+/Y	+/Y	+/Y	+/Y	+/N
F25	+/Y	+/Y	+/Y	+/Y	+/Y	+/Y	+/Y	+/Y	+/N	+/Y
F26	+/Y	+/Y	+/Y	+/Y	+/Y	+/Y	−/N	+/Y	+/Y	+/Y
F27	+/Y	+/Y	+/Y	+/Y	+/Y	+/Y	+/Y	+/Y	+/N	−/N
F28	+/Y	+/Y	+/Y	+/Y	+/Y	+/Y	+/Y	+/Y	+/N	+/Y
F29	+/Y	+/Y	+/Y	+/Y	+/Y	+/Y	+/Y	+/Y	+/Y	+/Y

only to the MBA and WOA. (T_0 = 0.01834 s, T_1 = 0.3819 s in 10D, T_1 = 0.5102 s in 30D and T_1 = 0.8274 s in 50D.)

3.4. Modified LWIFCM clustering algorithm based on the GPA

In this section, a modified LWIFCM clustering algorithm based on the GPA (GPA-LWIFCM) is proposed to optimize the key parameters of the LWIFCM and search the optimal initial clustering centers.

3.4.1. The implementation of the modified algorithm

The implementation process of the GPA-LWIFCM is as follows:

Step 1: Parameter settings. Set the parameters of the GPA: the total number of gold diggers (p), the maximum number of iterations (n), the subjective tolerance factor (k_w) and the dimensions of the search variables d (d = 2 in the GPA-LWIFCM). Meanwhile, set the maximum number of iterations N in the LWIFCM.

Step 2: Iterative optimization. Clustering centers c are produced and the fitness value of each center is calculated according to Eq. (27). When $\hat{J}$ (in Eq. (14)) reaches its smallest value, the fitness is at its maximum. The iterative process is conducted according to the GPA and a new clustering center is generated in each circulation:

$$fitness = \frac{1}{1 + \hat{J}(U, V)}, \tag{27}$$

Step 3: Termination iteration condition. If the iteration number reaches the maximum number of iterations n, the iteration process terminates, otherwise, continue.

Table 11
Results of the Fridman test for CEC'17.

	DPSO	FA	MBA	HHO	MFO	GWO	MVO	WOA	SSA	EBOwithCMAR	GPA
F1	9.24	11.00	7.31	9.71	5.24	5.55	3.61	6.41	3.00	3.76	1.18
F2	8.47	10.53	5.31	9.24	7.19	7.31	4.31	6.71	1.42	3.31	2.20
F3	9.02	10.84	4.64	9.73	6.57	6.79	3.82	6.98	4.39	1.08	2.14
F4	9.14	9.90	10.43	8.08	5.94	3.61	3.47	6.96	3.92	3.29	1.25
F5	8.73	9.20	10.82	8.80	4.43	1.84	1.92	7.41	4.10	4.37	4.37
F6	8.47	7.76	11.00	9.47	5.33	4.39	4.08	7.98	3.57	2.36	1.59
F7	8.41	7.37	10.96	8.39	7.14	3.80	3.47	8.04	4.27	2.69	1.45
F8	8.16	8.61	11.00	8.67	6.84	5.06	3.25	7.12	3.54	1.26	2.49
F9	8.88	10.37	8.39	7.73	6.08	2.76	3.18	6.14	3.80	6.67	2.00
F10	8.33	11.00	7.98	8.92	6.25	4.37	2.43	6.57	4.98	3.08	2.08
F11	3.16	10.90	7.00	9.08	5.00	6.47	4.14	8.10	6.45	3.94	1.76
F12	6.48	11.00	7.36	5.36	5.98	5.86	2.63	4.88	4.64	9.81	2.00
F13	6.16	11.00	6.67	7.08	9.31	6.06	2.82	6.98	4.43	3.28	2.22
F14	5.24	11.00	7.14	9.02	8.43	6.41	1.31	7.37	4.53	3.80	1.75
F15	7.78	10.53	9.69	7.65	6.24	4.73	4.84	6.18	2.92	3.20	2.25
F16	7.47	8.39	10.73	7.63	6.47	4.08	4.16	5.78	4.16	5.90	1.24
F17	2.49	11.00	8.20	5.47	7.35	7.33	5.16	6.27	6.55	4.63	1.55
F18	5.02	11.00	5.45	9.00	7.90	5.31	1.02	8.76	3.47	5.82	3.24
F19	8.10	10.23	10.33	7.49	4.84	3.80	4.28	5.40	3.43	6.94	1.16
F20	7.96	11.00	9.71	6.86	6.31	4.61	4.43	5.63	2.96	3.98	2.55
F21	8.35	10.49	9.78	8.31	5.61	4.71	4.59	6.24	4.31	2.15	1.46
F22	9.16	11.00	9.37	8.06	5.94	3.47	3.88	6.41	3.49	2.69	2.53
F23	3.00	10.98	9.73	7.61	5.59	3.55	3.84	5.92	3.18	8.20	4.41
F24	8.94	11.00	4.75	9.55	6.39	4.69	3.82	5.98	4.63	3.35	2.90
F25	8.16	10.33	9.82	8.25	5.22	4.43	3.98	6.67	2.56	4.08	2.50
F26	8.27	11.00	8.73	9.12	4.37	4.67	2.04	6.86	2.76	6.04	2.14
F27	5.49	11.00	5.83	8.88	7.10	7.27	6.12	7.31	3.16	1.45	2.38
F28	8.71	11.00	9.24	7.96	5.76	3.76	4.00	6.98	2.69	3.51	2.39
F29	4.39	11.00	3.02	9.27	7.25	6.88	6.43	7.45	5.45	3.27	1.57
AVG	7.28	10.36	8.29	8.29	6.28	4.95	3.69	6.74	3.89	4.07	2.16

Table 12
Algorithm complexity of the DPSO, FA, MBA, HHO, MFO, GWO, MVO, WOA, SSA, EBOwithCMAR and GPA.

		DPSO	FA	MBA	HHO	MFO	GWO	MVO	WOA	SSA	EBOwithCMAR	GPA
$\hat{T}_2$	D10	2.83	5.64	2.45	6.32	2.60	2.60	2.93	2.51	2.76	3.21	2.61
	D30	2.80	5.61	2.44	6.23	2.60	2.58	2.92	2.52	2.76	2.79	2.59
	D50	3.29	6.13	2.95	6.82	3.10	3.07	3.40	3.02	3.25	3.70	2.96
$\frac{(\hat{T}_2-T_1)}{T_0}$	D10	133.44	286.51	112.50	323.54	120.96	120.79	139.01	116.05	129.68	154.33	121.38
	D30	124.86	278.10	104.96	311.80	114.07	112.87	131.14	109.65	122.41	124.16	113.36
	D50	134.51	289.16	115.75	326.73	123.65	122.02	140.29	119.40	132.05	156.63	116.47

The pseudo-code of the modified LWIFCM clustering algorithm based on the GPA is shown in Algorithm 2, and the flowchart can be shown in Fig. 4.

Algorithm 2 The pseudo-code of the GPA-LWIFCM

```
Read the image to be processed, and initialize p, n, d, k_w, N;
Generate original clustering center V, m and α of LWIFCM, calculate the best_fitness;
N_iter = 1;
while (N_iter ≤ n)
    Update clustering center V, m and α of the LWIFCM according to Eqs. (23)–(25);
    j=1;
    while (j ≤ N)
        Update clustering center V and membership degree U;
    end while
    Calculate fitness according to Eq. (27);
    if fitness ≤ best_fitness
        Update the best_fitness, best clustering center V, best m, and best α;
        Set N_iter=N_iter+1;
    else set N_iter=N_iter+1;
    end if
end while
Importing the optimal value into the LWIFCM;
Output segmentation results;
```

3.4.2. Evaluation of the proposed image segmentation algorithms

The synthetic images are widely used as the sample data in evaluating image segmentation methods, because they are easy to acquire and the processed results can be evaluated intuitively (Lei et al., 2018; Wan et al., 2018). In this section, three different types of images are used to evaluate the performance of the GPA-LWIFCM, including the synthetic images with different noises, the multi-gray synthetic images with different noises, and the synthetic images with non-uniform Gaussian noises. In this experiment, five other fuzzy clustering algorithms are selected for comparison, as follows: the FCM_S1 and FCM_S2 (Chen and Zhang, 2004), the fast generalized fuzzy c-means (FGFCM) algorithm (Cai et al., 2007), the fuzzy local information c-means (FLICM) algorithm (Krinidis and Chatzis, 2010) and the FCM clustering algorithm based on the EBO (EBO–FCM) algorithm (Zhang et al., 2017). Besides, the LWIFCM clustering algorithm based on the MVO (MVO-LWIFCM) is also used as a comparison, because the MVO has an excellent performance in the previous section. The parameter settings are as follows: the maximum number of iterations $N = 50$ and the number of cluster centers $c = 4$ for each algorithm, and the fuzzifier constant $m = 2$ except the EBO–FCM, MVO-LWIFCM, and GPA-LWIFCM. Furthermore, the window sizes are set to 3×3 in the FLICM, LWIFCM, MVO-LWIFCM and GPA-LWIFCM. The parameters of the EBO-FCM are set as suggested in the Zhang et al. (2017). For the MVO-LWIFCM and GPA-LWIFCM, the iteration times n is set to 50, the colony size $p = 10$, and the subjective tolerance factor k_w of the GPA is set to 13.

The performance of each algorithm is evaluated by the similarity index (ρ) (Zijdenbos and Dawant, 1994) between the optimal segmented

Fig. 4. Flowchart of the GPA-LWIFCM.

image and fuzzy segmented image:

$$\rho = \frac{2\left|X_i \cap O_i\right|}{\left|X_i\right| + \left|O_i\right|}, \tag{28}$$

where O_i denote the pixels that belong to the optimal segmented image, X_i denote the pixels that belong to the fuzzy segmented image by mentioned methods, and $\left|X_i\right|$ and $\left|O_i\right|$ denotes the cardinality of X_i and O_i, respectively.

Each kind of synthetic images is generated 51 times independently, and the generated images are utilized as the samples for the image segmentation method evaluation. For each kind of synthetic image, all 51 similarity indexes were collected, and the optimal and average similarity index were recorded in Table 13 (In each cell, the optimal and average value are recorded at the top and bottom, respectively), and the segmented images with the optimal similarity indexes are shown in Figs. 5, 7 and 8. Moreover, in order to reflect the performance of the segmentation method more intuitively, the statistical analysis results are shown in Figs. 6 and 9.

From Table 13, except for the image segmentation method based on iteration, the optimal similarity index of the LWIFCM is significantly higher than that of other algorithms for the image with Gaussian noise. For salt and pepper noise, the LWIFCM is better than the FCM-S1, FGFCM, and FLICM in similarity index, but worse than the FCM-S2, FGFCM, EBO-FCM, MVO-LWIFCM, and GPA-LWIFCM. The reason why the LWIFCM is less effective than FCM-S2 in dealing with salt and pepper noise can be explained as follows: In the FCM-S2, the original sample point is replaced with the medium value of its around points, and this change show a strong advantage in dealing with pulse noise, whose principle is the same as median filtering. However, such replacement in the FCM-S2 loses the membership-degree information of the original sample points, which is not conducive to the correct division of the image, resulting in greater limitations of the algorithm. For the FGFCM, although the optimal similarity index is larger than the LWIFCM, the quality of image segmentation fluctuates greatly.

For the other two types of images, the optimal similarity indexes of the LWIFCM are superior to other segmentation methods except for the EBO-FCM, MVO-LWIFCM, and GPA-LWIFCM. The reasons for this phenomenon are as follows: First, due to the introduction of local information, the algorithm has an excellent ability to suppress noise, which is inherited from the FLICM. Second, the LWIFCM balances the relationship among local information, original membership degree, and intuitive membership degree by introducing local information weight, which enhances the interpretation ability of uncertain points and noise suppression ability. The introduction of local information weight makes the fuzzy membership degrees play a more important and decisive role in low noise areas. Correspondingly, local information plays a decisive role in high noise areas.

Table 13
Similarity indexes of the synthetic square images with different noises.

Methods		FCM_S1	FCM_S2	FGFCM	FLICM	LWIFCM	EBO-FCM	MVO-LWIFCM	GPA-LWIFCM
Gaussian	Opt.	79.13	79.11	69.66	85.12	86.17	88.14	89.23	**89.37**
(5%)	AVG	78.51	78.31	64.08	84.38	85.51	87.84	88.23	**89.11**
Gaussian	Opt.	67.02	68.23	60.16	70.62	70.91	70.95	**70.96**	**70.96**
(10%)	AVG	64.03	67.57	54.68	70.08	70.29	70.30	70.12	**70.34**
Salt & pepper	Opt.	90.70	**96.24**	94.06	87.64	87.93	92.63	94.11	94.49
(5%)	AVG	90.33	**96.19**	91.92	83.75	87.54	89.70	90.89	92.19
Salt & pepper	Opt.	82.46	**93.42**	91.97	77.83	77.83	84.72	85.70	85.70
(10%)	AVG	81.91	**93.14**	84.15	76.91	77.08	84.33	85.18	85.38
Multi-gray	Opt.	84.24	83.29	79.88	89.37	90.88	91.00	**91.01**	**91.05**
(10%)	AVG	83.88	80.31	74.22	86.71	87.09	90.44	89.97	**90.92**
Multi-gray	Opt.	81.03	80.51	75.10	87.65	88.44	89.48	**89.68**	**89.69**
(20%)	AVG	80.75	80.20	70.11	85.96	87.82	88.32	89.00	**89.07**
Non-uniform noise	Opt.	98.21	98.66	97.87	98.69	98.82	99.05	**99.23**	**99.23**
(0.1%, 0.5% and 1%)	AVG	97.91	98.11	95.25	96.84	98.07	99.04	99.04	**99.19**
Non-uniform noise	Opt.	87.52	88.61	87.37	88.17	89.76	95.64	**96.07**	**96.12**
(5%, 10% and 15%)	AVG	87.01	88.42	83.47	86.00	89.32	95.69	95.72	**95.91**

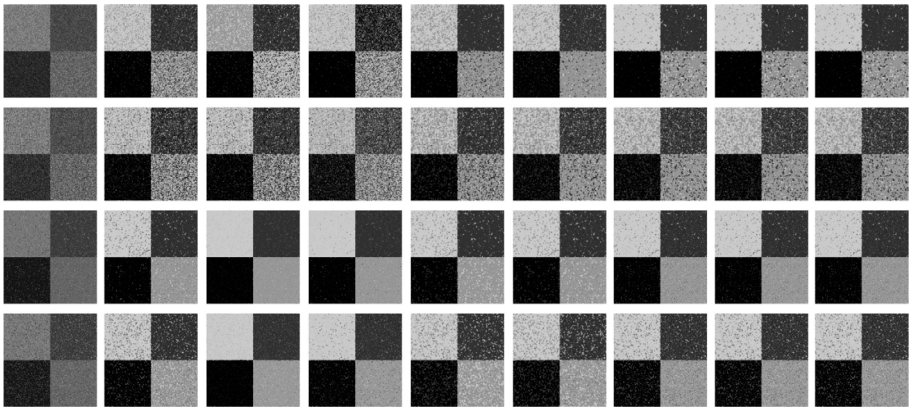

Fig. 5. Comparison of image segmentation results with different noises. Each row from top to bottom represents Gaussian (5%), Gaussian (10%), salt and pepper (5%) and salt and pepper (10%) noises, respectively. Each column from left to right represents the noisy images and the clustering results using the FCM_S1, FCM_S2, FGFCM, FLICM, LWIFCM, EBO-FCM, MVO-LWIFCM and GPA-LWIFCM, respectively.

It can be seen clearly from Figs. 6, 9, and Table 13 that the EBO-FCM, MVO-LWIFCM, and GPA-LWIFCM are superior to other algorithms in the similarity index. This is because both of them are based on iterative algorithms, which can adaptively select the initial clustering centers and have obvious advantages in improving the quality of image segmentation. The GPA-LWIFCM algorithm is superior to other algorithms in the segmentation quality for almost all images, followed by the MVO-LWIFCM. Compared with the MVO-LWIFCM, the better properties of the GPA-LWIFCM are obviously shown by the average results as shown in Table 13. Meanwhile, the GPA-LWIFCM also has better robustness than the MVO-LWIFCM, which can be seen from Figs. 6 and 9. When segmenting the synthetic images containing salt and pepper noise, the optimal similarity index of the FCM-S2 is higher than that of the GPA-LWIFCM, because the median filter is more suitable for processing pulse noise.

In conclusion, compared with other algorithms, the LWIFCM has a higher probability to obtain better image segmentation results for different noisy images. The introduction of the GPA optimizes the selection of the initial clustering centers and key parameters and further enhances the image segmentation ability of the LWIFCM. The optimized LWIFCM algorithm (GPA-LWIFCM) shows higher accuracy and robustness in image segmentation, making it a competitive image segmentation algorithm.

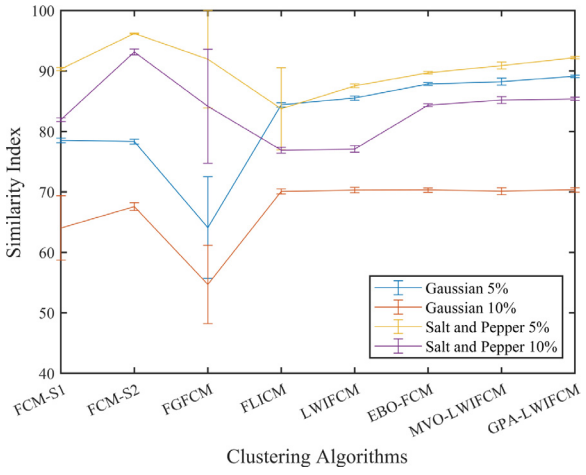

Fig. 6. The statistical analysis for similarity indexes of different clustering methods (images with the Gaussian noises or salt & pepper noises).

4. Application of the proposed algorithm

coal–rock interface recognition is one of the key problems to be solved in coal intelligent mining. In recent years, many scholars have put forward some solutions to this problem. Frederick L. D. (Frederick and Medley, 2002) detects coal–rock interface by natural gamma rays in rocks. Mowrey G. L. (Mowrey, 1991) uses crystals such as sodium iodide to make gamma-ray detectors and apply them to coal–rock interface recognition. Sahoo R. (Sahoo and Mazid, 2009) proposes using opto-tactile sensor to identify coal–rock interface, and develops related devices for shearer cutting drum height adjustment. Due to the limitations of the above methods in accuracy or robustness, etc., it is

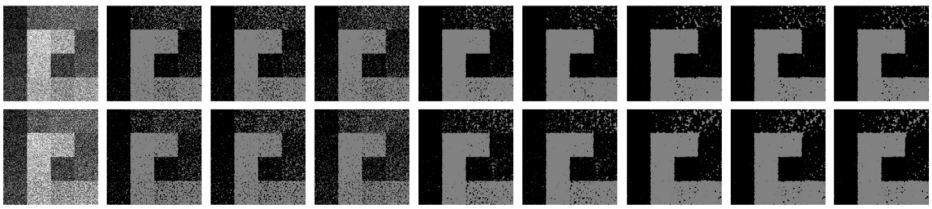

Fig. 7. Comparison of segmentation results for multi-gray block images. Each row from top to bottom represents the Gaussian (10%), Gaussian (20%) noises, respectively. The image segmentation method represented by each column is consistent with that in Fig. 5.

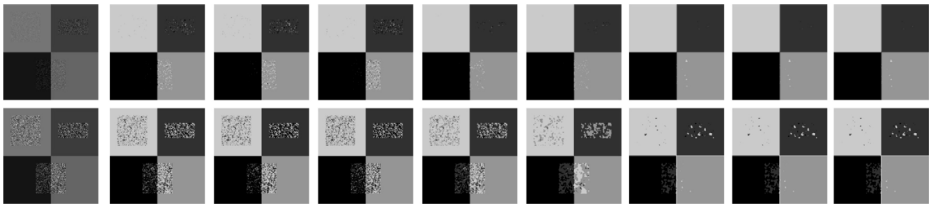

Fig. 8. Comparison of image segmentation results for images with non-uniform Gaussian noises. Each row from top to bottom represents the Gaussian (0.1%, 0.5% and 1%) and Gaussian (5%, 10% and 15%) noises, respectively. The image segmentation method represented by each column is consistent with that in Fig. 5.

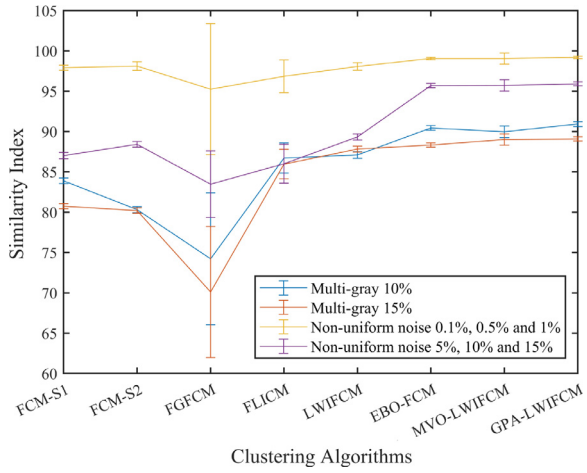

Fig. 9. The statistical analysis for similarity indexes of different clustering methods (images with multi-gray or non-uniform noises).

difficult to meet the requirement of the intelligent shearer control, so the recognition of the coal–rock interface is still an urgent problem in the field of coal intelligent mining. To solve this problem, many methods have been tried by us in recent years. Among them, infrared thermal imaging technology attracts our attention because of its strong penetration and high real-time performance. Because of the friction between cutting section and coal wall, the different hardness of coal–rock materials will show different temperature rise after cutting, and the temperature will not decrease significantly in a short time. It is considered to be an effective method to identify the coal–rock interface by using infrared temperature images of coal wall after cutting.

Firstly, the inherent complex noise in the infrared image is a problem that has to be solved when the infrared thermal imaging technology is applied. Secondly, the infrared thermal imagers use array thermosensitive units to detect and image the thermal radiation in space, but the performance of each thermosensitive unit is different in the actual imaging process, which causes the properties and intensity of noises are different in different parts of the obtained infrared image. Furthermore, the complex conditions of the fully mechanized coal face, including temperature, humidity, and the transmission of the long-distance industrial ring, amplify the above noise. Therefore, how to deal with the complex non-uniform infrared image noise has become one of the difficulties in solving the problem of coal–rock interface recognition. Since the running speed of the shearer is slow (usually 2–8 m/min) and the time span of two cutting at the same place is long, causing that it is possible to adopt a more stable image segmentation method. The image segmentation method proposed in this paper has been verified by the simulation above, showing a more stable ability to deal with multiple noises. Therefore, the coal–rock interface recognition experiment based on infrared thermal imaging technology had been designed and completed, and the clustering algorithm proposed in this paper was applied to segment infrared images, to realize the recognition of the coal–rock interface. The self-designed experiment system for shearer cutting coal–rock was built as Fig. 10. According to the structure of the shearer coal–rock cutting system, a reduced version cutting system was built to collect infrared image signals, including a single-drum cutting experimental platform, artificial coal–rock specimens, coal–rock specimen fixed platform, industrial ring, and so on. Artificial coal–rock specimens are composed of different proportions of coal, sand, cement, and binder, which are used to simulate different hardness coal–rock materials. They cannot fully reflect the coal–rock structure but as an approximate substitute. The coal–rock distribution in the fully mechanized coal face is much more complex. However, this method is mostly used in coal–rock cutting experiments to solve the problem that real coal–rock materials are difficult to obtain because of the limitation of the coal-mine underground environment and the requirement of mine safety production (Lei et al., 2019).

In this experiment, the shearer hauling speed was set to 5m/min to cut the artificial coal–rock specimen, and the coal-wall infrared images were collected as sample images of coal–rock interface recognition. The specimen consists of three cylindrical granites, two soft mixtures: mixture ratio (coal, sand, and cement) is 2:1:1, and two different base mixtures: mixture ratios (coal, sand, and cement) are 1:1:1 and 1.5:1:1. The obtained infrared image is shown in Fig. 11. The hardness of the three materials decreased successively from granite, base mixture(1:1:1), base mixture(1.5:1:1), and soft mixture. Finally, in order to evaluate the segmentation results more comprehensively, the traditional FCM, FLICM, EBO-FCM, MVO-LWIFCM, and proposed GPA-LWIFCM are used to complete the fuzzy segmentation of the infrared image samples, and the experimental results are recorded, as shown in Fig. 12.

It can be seen from Fig. 12 that three different hardness regions in the artificial coal–rock specimen are effectively divided by different methods, but there are some differences in segmentation results. The FCM encounters difficulties in processing complex noises, and there was obvious residual noise on the right part of the processed image.

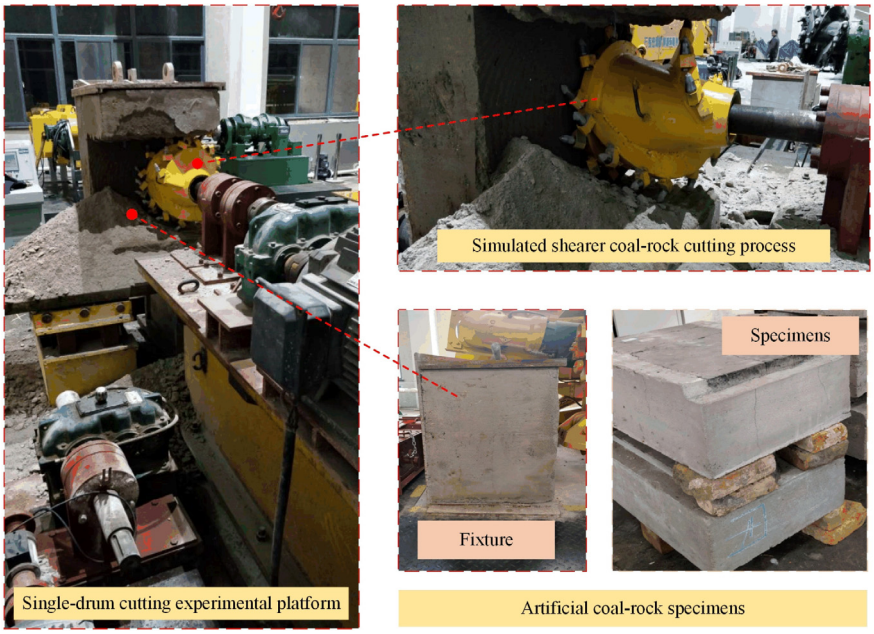

Fig. 10. Shearer cutting coal–rock experiment system.

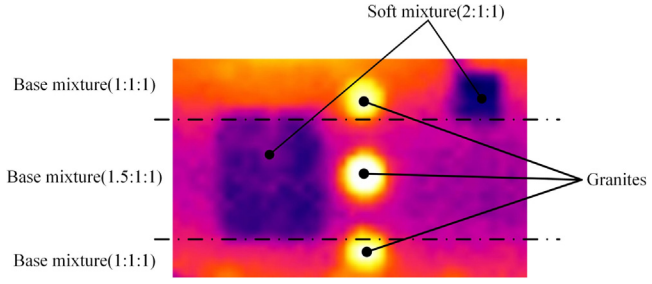

Fig. 11. Infrared image of the artificial coal–rock specimen.

The FCM cannot solve such difficulties. Even if the swarm intelligence algorithm is introduced, it is difficult to eliminate the noise influence on clustering results, as can be proved in Fig. 12(d). As shown in Fig. 12(b), the FLICM performs relatively insensitive to infrared noise, but the performance is limited due to the existence of non-uniform noise. Compared with the results of the proposed LWIFCM, the effects of the FLICM is not equally effective for non-uniform noises at different image parts, which causes the FLICM-based image segmentation results are poorer than the LWIFCM-based ones.

By introducing the MVO and GPA, the image segmentation performances have been further improved in robustness. As shown in Fig. 12(e,f), the transition between different regions becomes more stable, which is caused by selecting the cluster centers through iteration. Furthermore, as shown in Fig. 13, compared with the method based on the MVO-LWIFCM, the GPA-LWIFCM has better stability, specifically as follows: in 50 independent operations, 27 residual noise points appear in the red circle of the segmentation results based on the MVO-LWIFCM, but the same residual noise points do not appear in the segmentation results based on the GPA-LWIFCM. In summary, with the help of infrared thermal imaging technology, the proposed fuzzy image clustering algorithm can distinguish the coal–rock regions with different hardness well, to realize coal and rock interface recognition. The experiment proves that the proposed algorithm has application value and application space in practical engineering.

5. Conclusions and future work

In this paper, an intuitionistic fuzzy C-means clustering algorithm based on local information weights (LWIFCM) is proposed to realize the fuzzy segmentation. By introducing local information weight, the LWIFCM balances the role of fuzzy membership degrees and local information in fuzzy decision-making, to provide a more reasonable explanation for uncertain data. Meanwhile, a novel swarm intelligence algorithm (GPA) is proposed as a supplement to the LWIFCM. The application of the GPA further enhances the adaptability of the fuzzy clustering algorithm in image segmentation. In the GPA, each individual can independently make decisions on their subsequent behaviors in each iteration, which makes the algorithm show excellent local optimization ability. The existence of the local exploration further strengthens this ability. Meanwhile, the existence of the wealth tolerance factor further increases the global optimization ability of the algorithm, so that the algorithm keeps the ability to break away from the local optimization in the whole optimization process. Compared with the other optimization algorithms, the comparison times of the GPA obtaining significant optimal solution accounted for about 91.22% of the total comparison times. Based on the two proposed algorithms, this paper proposes the GPA-LWIFCM clustering method, which adaptively optimizes the key parameters and initial clustering centers. The proposed algorithm eliminates man-made parameter adjustment, further strengthens the processing ability for sample data, is well applied in image fuzzy segmentation. For 8 kinds of synthetic images, the average segmentation accuracy of the GPA-LWIFCM is 89.11%, 70.34%, 92.19%, 85.38%, 90.92%, 89.07%, 99.19%, and 95.91%, respectively, which is superior to most of the mentioned clustering methods.

In this paper, the proposed methods are applied to the coal–rock interface recognition, which effectively distinguishes the different hardness regions of the coal wall and obtains the coal–rock interface, further verifying its effectiveness in the processing of actual image segmentation. The preliminary experiments are shown in this paper to prove that the proposed method can be effectively applied to solve the problem of coal–rock interface recognition. In the future work, we will further improve the proposed methods, build an effective coal–

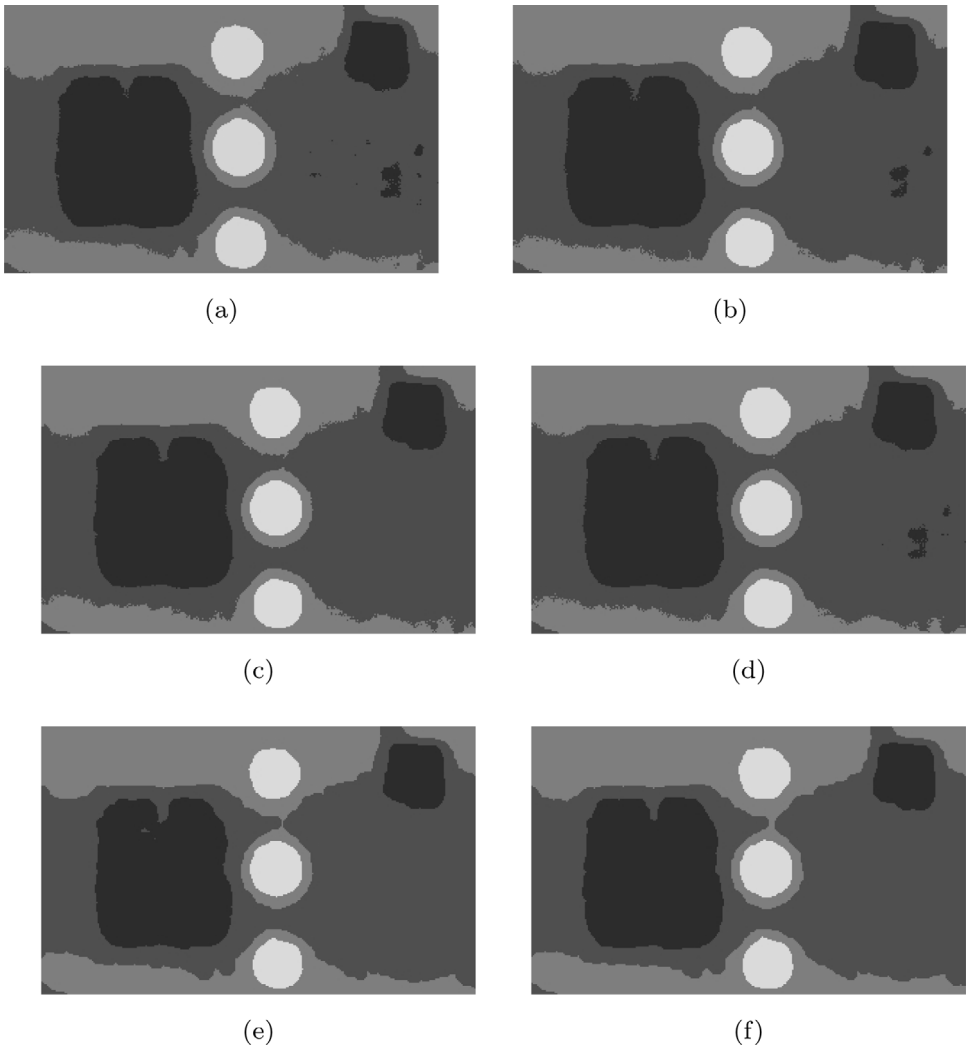

Fig. 12. Results of coal–rock interface recognition. (a) FCM; (b) FLICM; (c) LWIFCM; (d) EBO-FCM; (e) MVO-LWIFCM; (f) GPA-LWIFCM.

Fig. 13. Comparison between the image segmentations results based on the MVO-LWIFCM and GPA-LWIFCM, respectively. (a) MVO-LWIFCM; (b) GPA-LWIFCM.

rock interface recognition system, and hope the system can be applied to practice engineering projects in the field of coal-mine equipment intelligence in the future.

CRediT authorship contribution statement

Dong Wei: Conceptualization, Methodology, Formal analysis, Writing - original draft, Writing - review & editing. **Zhongbin Wang:** Conceptualization. **Lei Si:** Formal analysis. **Chao Tan:** Investigation, Data curation. **Xuliang Lu:** Investigation, Data curation.

Declaration of competing interest

The authors declare that they have no known competing financial interests or personal relationships that could have appeared to influence the work reported in this paper.

Acknowledgments

The authors would like to thank all of the reviewers for their constructive comments. The supports of National Natural Science Foundation of China (No. 52074271 and U1510117), National Key

Research and Development Program of China (No. 2020YFB1314200), China Postdoctoral Science Foundation (No. 2019M661974 and 2020T130696), and the Priority Academic Program Development (PAPD) of Jiangsu Higher Education Institutions China in carrying out this research are gratefully acknowledged.

References

Ahmed, M.N., Yamany, S.M., Mohamed, N., 2002. A modified fuzzy c-means algorithm for bias field estimation and segmentation of MRI data. IEEE Trans. Med. Imaging 21 (3), 193–199.

Atanasov, K., 1986. Intuitionistic Fuzzy Sets. Fuzzy Sets and Systems 20 (1), 87–96.

Bai, X., Chen, Z., Zhang, Y., Liu, Z., Lu, Y., 2016. Infrared Ship Target segmentation based on spatial information improved FCM. IEEE Trans. Cybern. 46 (12), 3259–3271.

Bezdek, J.C., 1981. Pattern Recognition with Fuzzy Objective Function Algorithms. Plenum Press.

Cai, W., Chen, S., D., Zhang., 2007. Fast and robust fuzzy c-means clustering algorithms incorporating local information for image segmentation. Pattern Recognit. 40 (3), 825–838.

Chen, S., Zhang, D., 2004. Robust image segmentation using FCM with spatial constraints based on new kernel-induced distance measure. IEEE Trans. Syst. Man Cybern. 34 (4), 1907–1916.

Chuang, K.S., Tzeng, H.L., Chen, S., Wu, J., Chen, T.J., 2006. Fuzzy c-means clustering with spatial information for image segmentation. Comput. Med. Imaging Graph. 30 (1), 9–15.

Dorigo, M., 1992. Optimization, Learning and Natural Algorithms (Ph.D. thesis). Politecnico di Milano, Italy.

Frederick, L.D., Medley, D., 2002. Armored rock detector[P], USA:US20020056 809A1, 2002-05-16.

Gonzales, R.C., Richard, E.W., 2010. Digital Image Processing, third ed. Prentice Hall, Upper Saddle River, N.J..

Gu, J., Jiao, L., Yang, S., Liu, F., 2017. Fuzzy double C-means clustering based on sparse self-representation. IEEE Trans. Fuzzy Syst. 99, 1.

Heidari, A.A., Mirjalili, S., Faris, H., et al., 2019. Harris hawks optimization: Algorithm and applications. Future Gener. Comput. Syst. 97 (AUG.), 849–872.

Ichihashi, H., Honda, K., Notsu, A., Ohta, K., 2008. Fuzzy c-means classifier with particle swarm optimization. In: 2008 IEEE International Conference on Fuzzy Systems (IEEE World Congress on Computational Intelligence). Hong Kong, pp. 207–215.

Jing, X., Zhongbin, W., Chao, T., et al., 2016. Adaptive wavelet threshold denoising method for machinery sound based on improved fruit fly optimization algorithm. Appl. Sci. 6 (7), 199.

Jing, X., Zhongbin, W., Chao, T., et al., 2018. Cutting pattern identification for coal mining shearer through a swarm intelligence–based variable translation wavelet neural network. Sensors 18 (2), 382.

Karaboga, D., 2010. Artificial Bee Colony Algorithm. Scholarpedia.

Kaufmann, A., 1980. Introduction to the Theory of Fuzzy Subsets: Fundamental Theoretical Elements-1. Academic Press, New York.

Kennedy, J., Eberhart, R., 1995. Particle swarm optimization. In: Proceedings of IEEE International Conference on Neural Networks. IV. pp. 1942–1948.

Khan, S.A., Mahmood, A., 2019. Fuzzy goal programming-based ant colony optimization algorithm for multi-objective topology design of distributed local area networks. Neural Comput. Appl. 31 (7), 2329–2347.

Krinidis, S., Chatzis, V., 2010. A robust fuzzy local information c-means clustering algorithm. IEEE Trans. Image Process. Publ. IEEE Signal Process. Soc. 19 (5), 1328–1337.

Kumar, A., Misra, R.K., Singh, D., 2017. Improving the local searchcapability of effective butterfly optimizer using covariance matrix adaptedretreat phase. In: 2017 IEEE Congress on Evolutionary Computation(CEC). IEEE, pp. 1835—1842.

Lei, T., Jia, X., Zhang, Y., He, L., Meng, H., Nandi, A.K., 2018. Significantly fast and robust fuzzy C-Means Clustering Algorithm based on morphological reconstruction and membership filtering. IEEE Trans. Fuzzy Syst. 26 (5), 3027–3041.

Lei, S., Zhongbin, W., Xinhua, L., Chao, T., 2019. A sensing identification method for shearer cutting state based on modified multi-scale fuzzy entropy and support vector machine. Eng. Appl. Artif. Intell. 78, 86–101.

Liu, Z.H., Wei, H.L., Zhong, Q.C., et al., 2016. Parameter estimation for VSI-Fed PMSM based on a dynamic PSO with learning strategies. IEEE Trans. Power Electron. 32 (4), 3154–3165.

Lloyd, S.P., 1982. Least squares quantization in PCM. IEEE Trans. Inform. Theory 28 (2), 129–137.

Mignotte, M., 2008. Segmentation by fusion of histogram-based K-means Clusters in Different Color Spaces. IEEE Trans. Image Process. 17 (5), 780–787.

Mirjalili, S., 2015. Moth-flame optimization algorithm: A novel nature-inspired heuristic paradigm. Knowl.-Based Syst. 89, 228—249.

Mirjalili, S., Amir, H., Gandomi, Mirjalili, S.Z., Saremi, S., Faris, H., Mirjalili, S.M., 2017. Salp Swarm Algorithm: A bio-inspired optimizer for engineering design problems. Adv. Eng. Softw. 114, 163–191.

Mirjalili, S., Lewis, A., 2016. The Whale Optimization Algorithm. Adv. Eng. Softw. 95, 51–67.

Mirjalili, S., Mirjalili, S.M., Hatamlou, A., 2016. Multi-Verse Optimizer: a nature-inspired algorithm for global optimization. Neural Comput. Appl. 27 (2), 495–513.

Mirjalili, S., Mirjalili, S.M., Lewis, A., 2014. Grey Wolf Optimizer. Adv. Eng. Softw. 69, 46–61.

Mowrey, G.L., 1991. Horizon control holds key to automation. Coal 11, 44–49.

Pan, W.T., 2012. A new Fruit Fly Optimization Algorithm: Taking the financial distress model as an example. Knowl. Based Syst. 26, 69–74.

Pan, W.T., 2013. Using modified fruit fly optimisation algorithm to perform the function test and case studies. Connect. Sci. 25, 151–160.

Pan, W.T., 2014. Mixed modified fruit fly optimization algorithm with general regression neural network to build oil and gold prices forecasting model. Kybernetes 43, 1053–1063.

Passino, K.M., 2002. Biomimicry of bacterial foraging for distributed optimization and control. IEEE Control Syst. 22 (3), 52–67.

Qi, X., Zhu, S., Zhang, H., 2017. A hybrid firefly algorithm. In: Proceedings of 2017 IEEE 2nd Advanced Information Technology. Electronic and Automation Control Conference, IAEAC 2017. pp. 287–291.

Saad, A., Dong, Z.M., Buckham, B., Crawford, C., Younis, A., Karimi, M., 2019. A new kriging-bat algorithm for solving computationally expensive black-box global optimization problems. Eng. Optim. 51 (2), 265–285.

Sahoo, R., Mazid, A.M., 2009. Application of opto-tactile sensor in shearer machine design to recognise rock surfaces in underground coal mining. In: IEEE International Conference on Industrial Technology. pp. 1–6.

Szilagyi, L., Benyo, Z., Szilagyi, S.M., 2003. MR brain image segmentation using an enhanced fuzzy C-means algorithm. In: Proceeding of the annual international conference of The IEEE Engineering in Medicine and Biology Society. pp. 724-726.

Szmidt, E., Kacpryzk, J., 2001. Entropy of an intuitionistic fuzzy set. Fuzzy Sets and Systems 118, 467–477.

Tanweer, M.R., Suresh, S., Sundararajan, N., 2015. Self regulating particle swarm optimization algorithm. Inform. Sci. 294, 182–202.

Tsai, P.W., Pan, J.S., Liao, B.Y., Tsai, M.J., Istanda, V., 2012. Bat algorithm inspired algorithm for solving numerical optimization problems. Appl. Mech. Mater. 148-149, 134–137.

Verma, H., Agrawal, R.K., Sharan, A., 2016. An improved intuitionistic fuzzy c-means clustering algorithm incorporating local information for brain image segmentation. Appl. Soft Comput. 46 (C), 543–557.

Wan, L., Zhang, T., Xiang, Y., You, H., 2018. A robust Fuzzy C-Means Algorithm based on Bayesian nonlocal spatial information for SAR image segmentation. IEEE J. Sel. Top. Appl. Earth Obs. Remote Sens. 11 (3), 896–906.

Wang, X.M., Hao, W.Q., Li, Q.M., 2017. An Adaptive Cultural Algorithm with improved quantum-behaved Particle Swarm Optimization for Sonar Image Detection. Sci. Rep. 7, 17733.

Xue, Y., Jiang, J.M., Zhao, B.P., Ma, T.H., 2018. A self-adaptive artificial bee colony algorithm based on global best for global optimization. Soft Comput. 22, 9.

Yager, R.R., 1980. On the measures of fuzziness and negation part II lattices. Inf. Control 44, 236–260.

Yang, Y., 2009. Image segmentation based on fuzzy clustering with neighborhood information. Opt. Appl. 39 (1), 135.

Yang, X.S., 2010a. Nature-Inspired Metaheuristic Algorithms, Nature-Inspired Metaheuristic Algorithms, second ed..

Yang, X.S., 2010b. A new metaheuristic Bat-Inspired Algorithm. Nature inspired cooperative strategies for optimization (NISCO 2010). Stud. Comput. Intell. 284, 65–74.

Zadeh, L.A., 1965. Fuzzy sets and systems. In: Proc of Symposium on Systems Theory. Polytechnic Institute of Brooklyn, NY, USA.

Zeshui, X., Junjie, W., 2010. Intuitionistic fuzzy C-means clustering algorithms. J. Syst. Eng. Electron. 21 (4), 580–590.

Zhang, M., Jiang, W., Zhou, X., et al., 2017. A hybrid biogeography-based optimization and fuzzy C-means algorithm for image segmentation. Soft Comput. 23 (1), 1–14.

Zhang, S., Wong, T.N., 2018. Integrated process planning and scheduling: an enhanced ant colony optimization heuristic with parameter tuning. J. Intell. Manuf. 29 (3), 585–601.

Zhide, L., Jiabin, C., Chunlei, S., 2009. A new RBF neural network with GA-based fuzzy C-means clustering algorithm for SINS fault diagnosis. In: 2009 Chinese Control and Decision Conference. Guilin, pp. 208–211.

Zijdenbos, A.P., Dawant, B.M., 1994. Brain segmentation and white matter lesion detection in MR images. Crit. Rev. Biomed. Eng. 22 (5–6), 401–465.